



Regular Article

Experimental Physics

Study of charmonium production via the decay to $p\bar{p}$ at $\sqrt{s} = 13$ TeV

LHCb Collaboration*

CERN, 1211 Geneva 23, Switzerland

Received: 25 July 2024 / Accepted: 10 October 2024
© CERN for the benefit of the LHCb collaboration 2024

Abstract Charmonium production cross-section in proton–proton collisions is measured at the centre-of-mass energy $\sqrt{s} = 13$ TeV using decays to $p\bar{p}$ final state. The study is performed using a data sample corresponding to an integrated luminosity of 2.2 fb^{-1} collected in 2018 with the LHCb detector. The production cross-section of the η_c meson is measured in a rapidity range of $2.0 < y < 4.0$ and in a transverse momentum range of $5.0 < p_T < 20.0\text{ GeV}/c$, which is extended compared with previous LHCb analyses. The differential cross-section is measured in bins of p_T and, for the first time, of y . Upper limits, at 90% and 95% confidence levels, on the $\eta_c(2S)$ and $h_c(1P)$ prompt production cross-sections are determined for the first time.

1 Introduction

In proton–proton (pp) collision events at the LHC, charmonium can originate from hadroproduction in a primary pp interaction vertex (PV) (referred to as “prompt production” hereafter) or from b -hadron decays in a vertex displaced from the PV by the flight distance of the b hadron (referred to as “from b -hadron”). In both cases, charmonium may also originate from decays of intermediate excited charmonium states (“feed-down”), whose contributions can only be subtracted when the production cross-section of the excited state and the probability of transition between the two charmonium states are known.

Despite a substantial theoretical effort, no consistent picture of the charmonium production mechanism is available [1]. Of the available approaches, nonrelativistic quantum chromodynamics (NRQCD) is the most successful in describing a wide range of measurements. It relies on three main assumptions. First, it assumes a factorisation between the perturbative process that creates a c quark and \bar{c} anti-quark, and the nonperturbative hadronisation of this pair into a charmonium meson. Second, it assumes the univer-

sality of the nonperturbative long-distance matrix elements (LDMEs), which considers, e.g., charmonium hadroproduction and production in b -hadron decays. Finally, the assumption of heavy-quark spin symmetry (HQSS) provides relations between LDMEs for the charmonium states with the same orbital and radial quantum numbers, e.g., the J/ψ and $\eta_c(1S)$ mesons.¹

The NRQCD calculations at next-to-leading order (NLO) successfully describe the observed production and polarisation of the J/ψ and $\psi(2S)$ states, but only in a limited range of charmonium transverse momentum p_T . A consistent description of the J/ψ hadro- and photo-production and polarisation, together with the production of the η_c meson, remains challenging [2]. The first measurement of the η_c meson production by the LHCb Collaboration [3] showed that the colour singlet (CS) contribution saturates the observed p_T -differential cross-section in the studied p_T region. This result led to a major revisiting of the theoretical framework and yielded new approaches capable of simultaneously describing the J/ψ and η_c production and J/ψ polarisation, albeit still within a limited p_T range [4]. The recent LHCb measurement of the η_c production [5] further constrains the theory and indicates a possible colour octet (CO) contribution at high p_T . Meanwhile, the theoretical prediction of Ref. [6] demonstrated the unphysical behaviour of the theoretical description at low p_T leading to negative total η_c production cross-section. The latter motivates a new measurement of η_c production at low p_T .

In order to confront the measured production cross-sections of the η_c and J/ψ mesons with theory, knowledge of the feed-down from excited states is needed. Instead, the authors of Ref. [7] proposed to measure the production of the first excited states, $\eta_c(2S)$ and $\psi(2S)$ mesons, free from feed-down contributions. The paper suggests the same relations between LDMEs as for the η_c and J/ψ states. In the same work, the authors predicted the $\eta_c(2S)$ hadroproduc-

*e-mail: valeriia.zhovkovska@cern.ch (corresponding author)

¹ The $\eta_c(1S)$ state is referred to as η_c throughout the paper.

tion cross-section in the LHCb acceptance at 13 TeV, based on three different sets of LDMEs from Refs. [8–10].

While $J^{PC} = 1^{--}$ charmonium states, J/ψ and $\psi(2S)$ mesons, are precisely studied thanks to their reconstruction in the experimentally clean dimuon decays, a simultaneous reconstruction of all known charmonium states is only possible via their decays to hadrons. In this paper, charmonium decays to $p\bar{p}$ are used, following previous studies done by the LHCb experiment [3, 5]. This decay is available for all charmonium states [11] and thus allows studying them simultaneously. The analysis covers prompt charmonium production and charmonium production in b -hadron decays of η_c , $\eta_c(2S)$, χ_{cJ} and $h_c(1P)$ states, using data collected by the LHCb experiment in 2018 corresponding to an integrated luminosity of 2.2fb^{-1} . The differential production cross-section of η_c is measured in four bins of rapidity, in the $2.0 < y < 4.0$ range, and in six p_T bins, in the $5.0 < p_T < 20.0\text{GeV}/c$ range, which extends that of Ref. [5]. Upper limits are set for the prompt $\eta_c(2S)$ and $h_c(1P)$ production cross-sections. The results also include the branching fractions of the χ_{cJ} production in inclusive b -hadron decays.

With its precise vertex reconstruction, powerful particle identification (PID) and flexible trigger, the LHCb experiment possesses excellent capabilities for charmonium production studies [3, 5, 12–19]. This suppresses a large combinatorial background contribution originating from the pp interaction. The present study exploits the 2018 data sample with a dedicated software trigger selection of $p\bar{p}$ combinations compatible with charmonium decays, in an extended range of invariant mass, transverse momentum and with reduced PID requirements compared to previous LHCb measurements [3, 5].

2 The LHCb detector and data sample

The LHCb detector [20, 21] is a single-arm forward spectrometer covering the pseudorapidity range $2 < \eta < 5$, designed for the study of particles containing b or c quarks. The detector includes a high-precision tracking system consisting of a silicon-strip vertex detector surrounding the pp interaction region, a large-area silicon-strip detector located upstream of a dipole magnet with a bending power of about 4 T m, and three stations of silicon-strip detectors and straw drift tubes placed downstream of the magnet. The tracking system provides a measurement of the momentum, p , of charged particles with a relative uncertainty that varies from 0.5% at low momentum to 1.0% at 200 GeV/ c . The minimum distance of a track to a primary pp collision vertex, the impact parameter (IP), is measured with a resolution of $(15 + 29/p_T)\mu\text{m}$. Different types of charged hadrons are distinguished using information from two ring-imaging Cherenkov (RICH) detectors. Photons, electrons

and hadrons are identified by a calorimeter system consisting of scintillating-pad and preshower detectors, an electromagnetic and a hadronic calorimeter. Muons are identified by a system composed of alternating layers of iron and multiwire proportional chambers.

The online event selection is performed by a trigger, which consists of a hardware stage based on information from the calorimeter and muon systems, followed by a software stage, which performs the charmonium candidate reconstruction. The hardware trigger selects events with a single high transverse energy deposit in the calorimeter. In addition, events with high multiplicity are rejected to reduce the number of random combinations of tracks (combinatorial background). The software stage then requires two oppositely charged tracks with a good track-fit quality, identified as protons. The studies of prompt charmonium decay to $p\bar{p}$ require a dedicated software trigger selection, which suffers from a large combinatorial background. To suppress the combinatorial background and reduce the trigger bandwidth, the proton tracks are required to have a transverse momentum larger than 2.0 GeV/ c , and a momentum larger than 12.5 GeV/ c . Charmonium candidates must have a good vertex quality and a transverse momentum larger than 5.0 GeV/ c . In between the two software stages, an alignment and calibration of the detector is performed in near real-time, and their results are used in the trigger [22]. The same alignment and calibration information is propagated to the offline reconstruction, ensuring consistent and high-quality tracking and particle-identification information in the trigger and offline software. The identical performance of the online and offline reconstruction offers the opportunity to perform physics analyses directly using candidates reconstructed in the trigger [23, 24], which the present analysis exploits. The storage of only the triggered candidates reduces the event size by an order of magnitude. The signal selection is largely performed at the trigger level. The only additional offline requirement is a tighter PID selection on the proton candidates. To account for imperfect knowledge of the magnetic field and tracker alignment, a momentum scale calibration [25] is applied to the data samples.

Simulation samples are used to model the effects of the detector acceptance and the imposed selection requirements. Generation of pp collision events is performed using the Pythia8 [26, 27] event generator with specific LHCb configuration [28]. Decays of hadronic particles are described by EvtGen [29], in which final-state radiation is generated using PHOTOS [30]. The interaction of generated particles with detector material is simulated using the GEANT4 package [31, 32].

For all simulation samples, the charmonium decay amplitude to $p\bar{p}$ is modelled to be uniform in the available phase space. The samples of J/ψ and $\psi(2S)$ mesons are simulated unpolarised. The samples of prompt η_c and $\eta_c(2S)$ are gener-

ated similarly to prompt J/ψ and $\psi(2S)$, respectively, with modified mass and width according to their known values from Ref. [11]. A sample of $J/\psi \rightarrow p\bar{p}\pi^0$ decays is generated to study the corresponding background contribution.

3 Cross-section determination

Measuring the ratios of the production cross-section of two charmonium states, a signal channel A and a normalisation channel B , allows for a partial cancellation of several systematic effects, and it can be expressed as

$$\frac{\sigma_A^X}{\sigma_B^X} = \frac{N_A^X}{N_B^X} \times \frac{\varepsilon_B^X}{\varepsilon_A^X} \times \frac{\mathcal{B}_{B \rightarrow p\bar{p}}}{\mathcal{B}_{A \rightarrow p\bar{p}}}, \quad (1)$$

where $X = p(b)$ for prompt production (production in b -hadron decays), σ^X is the production cross-section, N^X is the yield, and ε^X is the total efficiency to trigger, reconstruct and select the signal and normalisation modes of the charmonium candidates. The branching fractions $\mathcal{B}_{A(B) \rightarrow p\bar{p}}$ are taken from Ref. [11]. The ratio of branching fractions of the inclusive b -hadron decay to charmonium in Eq. 1 is obtained as the ratio of production cross-sections in b -hadron decays, $\frac{\mathcal{B}_{b \rightarrow AX}}{\mathcal{B}_{b \rightarrow BX}} = \frac{\sigma_b^A}{\sigma_b^B}$. The most precise determination of the J/ψ production cross-section [11, 15] is generally used to normalise the measurements.

The efficiency ε^X is determined as the product of the geometrical acceptance, trigger, reconstruction, particle identification and selection efficiencies. It is calculated using simulated samples separately for prompt charmonium and charmonium from b -hadron decays, and in each kinematic bin of the η_c meson for the differential production measurement. The hardware trigger and proton PID efficiencies are corrected using data-driven methods [33].

The prompt charmonium candidates (prompt sample) and charmonium candidates from b -hadron decays (b -decays sample) are separated using a pseudo-decay time

$$t_z = \frac{(z_d - z_p)M_{p\bar{p}}}{p_z}, \quad (2)$$

where z_p and z_d are the positions along the beam axis of the candidate production and decay vertex, respectively, $M_{p\bar{p}}$ is the reconstructed $p\bar{p}$ mass and p_z is the momentum component along the beam direction of a charmonium candidate. The prompt sample is selected by applying the requirement $t_z < 80$ fs, while the b -decays sample is obtained by requiring $t_z > 80$ fs and both proton tracks to be significantly displaced from any PV. The final result for the η_c production measurement is corrected for the cross-contamination between the prompt and b -decays samples. The correction is determined using the simulated samples, and it is calculated to be below 3% for the prompt sample and below 2% for the b -decays

sample. This correction for the other charmonium states is negligible compared to the statistical uncertainties.

4 Fits to data

4.1 Production cross-section of the $\eta_c(2S)$, $h_c(1P)$ and χ_{cJ} mesons

The yields of charmonium candidates are determined from a binned extended maximum-likelihood fit to the $p\bar{p}$ mass distribution in the range 2850–3750 MeV/ c^2 . The mass fit is performed simultaneously for the prompt and b -decays samples. Independent fits are performed for studies of the $\eta_c(2S)$ and $h_c(1P)$ prompt production, and χ_{cJ} production in inclusive b -hadron decays. The $J^{PC} = 1^{--}$ charmonium states, namely the J/ψ and $\psi(2S)$ mesons, have negligible natural width compared to the detector resolution, thus they are described by Crystal Ball functions representing the detector resolution. The other charmonium states are described by a convolution of a Crystal Ball function and a relativistic Breit–Wigner function. The J/ψ mass is a floating parameter and the η_c width is a fixed parameter in all fits. In the fits for the $\eta_c(2S)$ and $h_c(1P)$ prompt production study, masses of the η_c and $\psi(2S)$ states are freely varying parameters, while masses and natural widths of the $\eta_c(2S)$ and $h_c(1P)$ mesons are constrained to their known values [11] in the corresponding fits. The masses and widths of the χ_{cJ} states are fixed to their known values [11]. In the χ_{cJ} production measurement fit, masses of the χ_{c0} and χ_{c1} states are allowed to vary in the fit. Masses and widths of the other states except for the J/ψ meson are fixed to their known values [11]. Table 1 summarizes the parameterisation for different fits.

One common mass resolution parameter, σ_{CB} , is shared between the prompt and b -decays samples. The ratio of the mass resolution between each charmonium state and the J/ψ meson and the Crystal–Ball tail parameters are fixed according to the simulation. The combinatorial background is described by fourth- and third-order Chebyshev polynomial for the prompt and b -decays samples, respectively. Potential background contributions can be caused by $p\bar{p}$ combinations from other partially reconstructed charmonium decays. Only one such contribution arising from the $J/\psi \rightarrow p\bar{p}\pi^0$ decay, where the π^0 meson is not reconstructed, is considered in the fit. This background source can create a broad nonpeaking structure affecting the region below the η_c mass. In the fit, it is described by a square-root shape, $\sqrt{M_{J/\psi} - M_{\pi^0} - M_{p\bar{p}}}$, which is in good agreement with simulation. The normalisation of this background component is fixed to the J/ψ yield using known branching fractions of the $J/\psi \rightarrow p\bar{p}\pi^0$ and $J/\psi \rightarrow p\bar{p}$ decays [11], and the efficiency ratio between the two decay modes.

Table 1 Treatment of the parameters in the mass fits for the different studies. Parameters are fixed or constrained to their known values [11]

Fit	M_{η_c}	$M_{J/\psi}$	$M_{\chi_{c0}}$	$M_{\chi_{c1}}$	$M, \Gamma_{h_c(1P)}$	$M_{\chi_{c2}}$	$M, \Gamma_{\eta_c(2S)}$	$M_{\psi(2S)}$
$\eta_c(2S)$	Free	Free	Fixed	Fixed	Fixed	Fixed	Constrained	Free
$h_c(1P)$	Free	Free	Fixed	Fixed	Constrained	Fixed	Fixed	Free
χ_{cJ}	Fixed	Free	Free	Free	Fixed	Fixed	Fixed	Fixed

The $p\bar{p}$ mass distribution for the prompt and b -decays samples is shown in Fig. 1. Projections of the simultaneous fit result are overlaid. The yields of the charmonium states from the fit are listed in Table 2. The fit shows no significant $\eta_c(2S)$ and $h_c(1P)$ signals. Therefore, for these states, upper limits are set on the relative $\eta_c(2S)$ to J/ψ and $h_c(1P)$ to J/ψ production cross-section at 90% and 95% confidence levels (CL).

4.2 Differential production cross-section of the η_c meson

The η_c differential production cross-section measurement is performed in bins of the η_c transverse momentum and rapidity. To determine the ratio of the η_c to J/ψ yields, the fit to the $p\bar{p}$ mass distribution is performed simultaneously in bins of either p_T or y . The range of the mass fit is reduced to 2850–3250 MeV/ c^2 . The model of the signal description is the same as that for the fits described above. The dependency of the mass resolution on p_T and y is determined from simulation and scaled by a factor in the fit to data. The scaling parameter is obtained from a fit to the mass distribution in the simulated samples using the same signal parameterisation as that for data. The J/ψ mass and the mass difference between the J/ψ and η_c states are left as floating parameters in the fit. The combinatorial background is described by an exponential function multiplied by a second-order polynomial for both prompt and b -decays samples. The cross-contamination between the samples is estimated from simulation in bins of p_T and y , and used for correcting the yields of the charmonium states.

The relative η_c to J/ψ yield is extracted from the fit and listed in Tables 3 and 4 for p_T and y bins, respectively.

5 Systematic uncertainties

Alternative fit parameterisations for the signal and background are used to estimate systematic uncertainties on the production cross-section. For the study of the $\eta_c(2S)$ and $h_c(1P)$ prompt production, the systematic uncertainties are included in the upper limit using the discrete profiling method [34]. For the other measurements, the systematic uncertainties are estimated as a difference between the baseline fit and

the fit with the alternative parameterisation. The following systematic uncertainties are common for all measurements.

The uncertainty associated with the mass resolution description is estimated using an alternative fit where the sum of two Gaussian functions with parameters determined from simulation is used instead of the Crystal Ball function. The uncertainty related to the knowledge of the charmonium natural width is estimated in alternative fits where the natural width is varied within the world-average uncertainties [11]. The largest variation is taken as the systematic uncertainty. The uncertainty associated with the combinatorial background description is estimated using an alternative background parameterisation. In the studies of the $\eta_c(2S)$ and $h_c(1P)$ prompt production cross-section and χ_{cJ} production in inclusive b -hadron decays, the background is parametrised using an exponential function multiplied by a third- or a second-order polynomial function for prompt and b -decays samples, respectively. In addition, in the $\eta_c(2S)$ and $h_c(1P)$ prompt production study, a second parameterisation uses the product of a square-root function, an exponential function and a polynomial. A third-order polynomial is used for the prompt sample, and a second-order polynomial function is used for the b -decays sample. In the η_c production studies, an alternative background parameterisation with a third-order Chebyshev polynomial is used. The systematic uncertainty related to the contribution from $J/\psi \rightarrow p\bar{p}\pi^0$ decays is estimated by varying the value of the efficiency ratio $\varepsilon_{J/\psi \rightarrow p\bar{p}\pi^0} / \varepsilon_{J/\psi \rightarrow p\bar{p}}$ and the branching ratio $\mathcal{B}_{J/\psi \rightarrow p\bar{p}\pi^0} / \mathcal{B}_{J/\psi \rightarrow p\bar{p}}$ within their uncertainties.

The systematic uncertainty corresponding to the ratio of efficiencies of different charmonium states is estimated by varying its value by the uncertainty corresponding to the simulation sample sizes. The uncertainties associated with possible discrepancies between data and simulation are largely cancelled out in the efficiency ratio. The uncertainty related to the cross-contamination between the prompt and b -decays samples is estimated by modifying the corresponding yields by their uncertainties.

The effect of possible nonzero polarisation of the J/ψ meson is accounted for in the reconstruction efficiency. Weights are assigned to the simulated $J/\psi \rightarrow p\bar{p}$ events to reproduce the distributions corresponding to the polarisation parameter values of $\lambda_\theta = \pm 0.1$ [15].

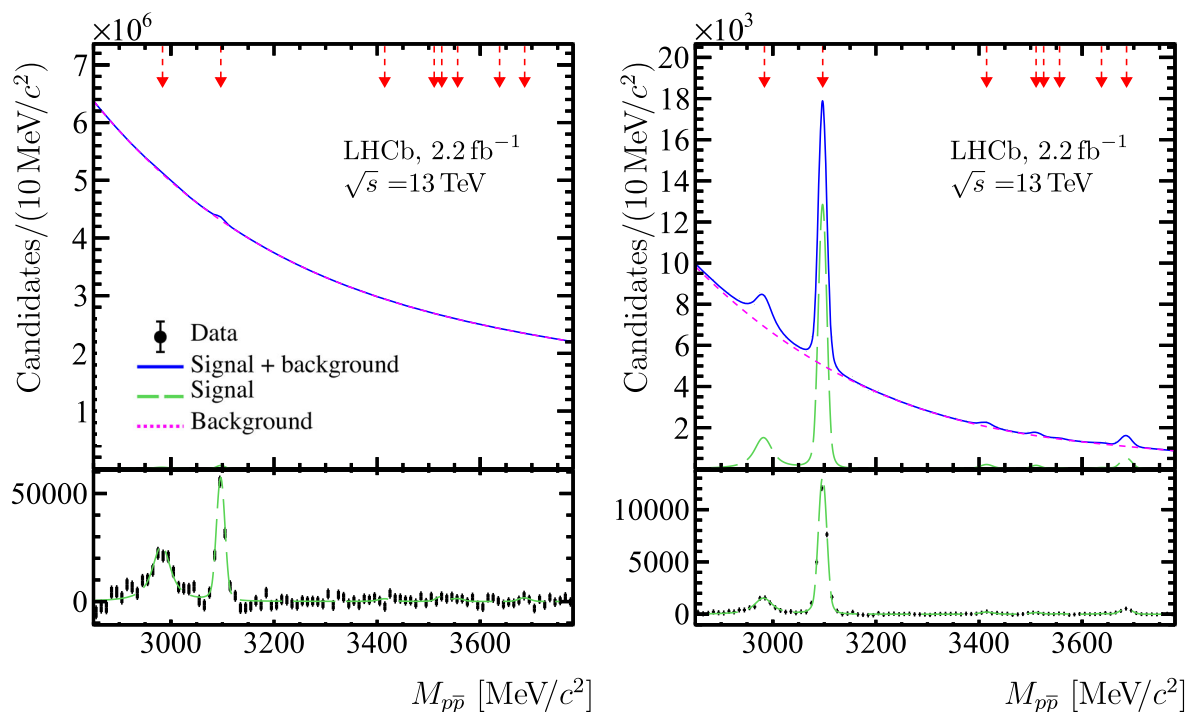


Fig. 1 Distribution of the $p\bar{p}$ mass for (left) prompt and (right) b -decays samples. The results of the fits using the configuration to study the $\eta_c(2S)$ prompt production are overlaid. Red arrows show invariant

mass of charmonium states in the following order: η_c , J/ψ , χ_{c0} , χ_{c1} , $h_c(1P)$, χ_{c2} , $\eta_c(2S)$ and $\psi(2S)$ states. The lower panel shows the data and the fit model with the background subtracted

Table 2 Results of the simultaneous fit to the $p\bar{p}$ mass distributions for combined prompt and b -decays data sample. Yields are restricted to be positive with symmetric uncertainties presented. The uncertainties are statistical only

Charmonium state	$N^p \times 10^2$	N^b	Mass [MeV/c ²]
η_c	1501 ± 99	8857 ± 361	2982.1 ± 0.8
J/ψ	1225 ± 42	27983 ± 248	3096.6 ± 0.1
χ_{c0}	47 ± 50	766 ± 136	3414.7
χ_{c1}	0 ± 62	443 ± 98	3510.7
$h_c(1P)$	63 ± 37	0 ± 67	3525.4
χ_{c2}	38 ± 39	125 ± 97	3556.2
$\eta_c(2S)$	0 ± 32	0 ± 52	3637.5
$\psi(2S)$	49 ± 37	1529 ± 91	3685.3 ± 0.8

The uncertainty of the efficiency ratios, as well as the uncertainties of the $\mathcal{B}_{J/\psi \rightarrow p\bar{p}}$ and $\mathcal{B}_{\eta_c \rightarrow p\bar{p}}$ values, are taken into account directly in the production cross-section determination. The systematic uncertainties on the signal yields are propagated to the production cross-section using Eq. 1.

The η_c differential production cross-section measurement includes the uncertainty corresponding to the p_T or y dependence of the relative mass resolution between η_c and J/ψ states. It is accounted for by introducing a linear dependence of the resolution as a function of p_T or y constrained by simulation. For the η_c differential production cross-section measurement, the systematic uncertainties on the combinatorial background description, resolution ratio, cross-contamination between samples and the contribution

Table 3 Ratios of the observed η_c to J/ψ yields corrected for cross-contamination for prompt production and production in b -hadron decays in bins of transverse momentum p_T . The uncertainties are statistical

p_T [GeV/c]	$N_{\eta_c}^p / N_{J/\psi}^p$	$N_{\eta_c}^b / N_{J/\psi}^b$
5.0–6.5	0.34 ± 0.32	0.295 ± 0.057
6.5–8.0	0.70 ± 0.21	0.247 ± 0.034
8.0–10.0	1.07 ± 0.15	0.302 ± 0.027
10.0–12.0	0.88 ± 0.20	0.358 ± 0.034
12.0–14.0	1.34 ± 0.29	0.318 ± 0.039
14.0–20.0	1.30 ± 0.42	0.313 ± 0.042
5.0–20.0	0.87 ± 0.09	0.303 ± 0.017

Table 4 Ratios of the observed η_c to J/ψ yields mesons corrected for cross-contamination for prompt production and production in b -hadron decays in bins of rapidity y . The uncertainties are statistical

y	$N_{\eta_c}^p/N_{J/\psi}^p$	$N_{\eta_c}^b/N_{J/\psi}^b$
2.0–2.5	0.64 ± 0.15	0.304 ± 0.027
2.5–3.0	1.12 ± 0.19	0.315 ± 0.027
3.0–3.5	0.86 ± 0.19	0.300 ± 0.029
3.5–4.0	0.83 ± 0.40	0.317 ± 0.066

Table 5 Relative uncertainties (in %) on the ratio of prompt cross-sections $\sigma_{\eta_c}^p/\sigma_{J/\psi}^p$. Uncertainties on $\mathcal{B}_{\eta_c \rightarrow p\bar{p}}$ and $\mathcal{B}_{J/\psi \rightarrow p\bar{p}}$ measurements are considered separately and given in the text

	p_T [GeV/c] 5.0–20.0
Statistical uncertainty	10.4
Combinatorial background	5.4
Contribution from $J/\psi \rightarrow p\bar{p}\pi^0$	0.3
Resolution p_T -dependence	0.1
Cross-feed	< 0.1
Total uncorrelated systematic	5.4
Variation of Γ_{η_c}	1.7
Mass resolution model	1.8
Polarisation of J/ψ	1.6
Total correlated systematic	3.0
Total systematic	6.2

from the $J/\psi \rightarrow p\bar{p}\pi^0$ decay are estimated bin-by-bin and considered as uncorrelated among bins. To reduce the impact of statistical fluctuations, they are smoothed over bins using a linear interpolation. The systematic uncertainties on the η_c natural width, mass-resolution model and J/ψ polarisation are considered as correlated among bins. The first two are estimated from the fit to the mass distribution in the entire p_T (y) range and assumed to be the same in all the bins. The uncertainties on the relative η_c prompt production cross-sections are given in Table 5. The uncertainties in bins of p_T and y are summarised in Tables 9 and 10 in the Appendix.

6 Results

6.1 Prompt production of the $\eta_c(2S)$ and $h_c(1P)$ mesons

The upper limits at 90% and 95% confidence level (CL) on the relative and absolute prompt production cross-section at $\sqrt{s} = 13$ TeV for the $\eta_c(2S)$ and $h_c(1P)$ states are set for the first time. The study is performed in the kinematic range $5.0 < p_T < 20.0$ GeV/c and $2.0 < y < 4.0$. The results are listed in Table 6 and shown in Figs. 2 and 3. The Bayesian approach [35] was used for setting the upper limits.

Table 6 Upper limits at 90% and 95% CL for the $\eta_c(2S)$ and $h_c(1P)$ prompt production cross-sections and their ratios to that of the J/ψ meson, extracted using a Bayesian approach

Upper limit	90% CL	95% CL
$(\sigma_{\eta_c(2S)} \times \mathcal{B}_{\eta_c(2S) \rightarrow p\bar{p}})/(\sigma_{J/\psi} \times \mathcal{B}_{J/\psi \rightarrow p\bar{p}})$	0.113	0.136
$\sigma_{\eta_c(2S)} \times \mathcal{B}_{\eta_c(2S) \rightarrow p\bar{p}}$ [nb]	0.331	0.401
$(\sigma_{h_c(1P)} \times \mathcal{B}_{h_c(1P) \rightarrow p\bar{p}})/(\sigma_{J/\psi} \times \mathcal{B}_{J/\psi \rightarrow p\bar{p}})$	0.117	0.133
$\sigma_{h_c(1P)} \times \mathcal{B}_{h_c(1P) \rightarrow p\bar{p}}$ [nb]	0.327	0.375

A comparison of the results for the $\eta_c(2S)$ production and an NLO NRQCD theoretical prediction [7] is shown in Table 7. The comparison is performed in different kinematic ranges due to the lack of J/ψ prompt production cross-section measurement in the same kinematic range as the current $\eta_c(2S)$ measurement. Therefore, an additional upper limit for the $\eta_c(2S)$ prompt production cross-section at 95% CL is set in the p_T range $5.0 < p_T < 14.0$ GeV/c. Assuming that the difference between the J/ψ prompt production cross-section values estimated in the kinematic range $5.0 < p_T < 14.0$ GeV/c and $5.0 < p_T < 20.0$ GeV/c is compatible with their uncertainty, the absolute $\eta_c(2S)$ production cross-section in both p_T ranges is estimated using the first value. The predictions are made using three different sets of LDMEs: Shao et al. [8], Gong et al. [9], and Bodwin et al. [10]. The upper limit is found to be considerably lower than the prediction based on Bodwin et al. [10]. The obtained cross-section upper limit is also below the prediction by Shao et al. [8], which, however, reports large theory uncertainties.

6.2 Production of the η_c meson

The differential production cross-section of the η_c meson is measured for both prompt charmonium production and production in inclusive b -hadron decays. Results are presented in an extended p_T range in comparison to the previous analysis [5]. The p_T -differential cross-section is measured in the range $5.0 < p_T < 20.0$ GeV/c, and y -differential cross-section is measured for the first time in the range $2.0 < y < 4.0$.

Using Eq. 1 and yields extracted from the fit to data, the relative η_c to J/ψ prompt production cross-section is measured to be

$$\begin{aligned} & (\sigma_{\eta_c}/\sigma_{J/\psi})^{5.0 < p_T < 20.0 \text{ GeV/c}, 2.0 < y < 4.0} \\ & = 1.32 \pm 0.14 \pm 0.09 \pm 0.13. \end{aligned}$$

Here and throughout the paper, unless explicitly mentioned, the first uncertainty is statistical, the second is systematic, and the third is due to the uncertainties on the branching fractions $\mathcal{B}_{\eta_c \rightarrow p\bar{p}}$ and $\mathcal{B}_{J/\psi \rightarrow p\bar{p}}$.

The prompt J/ψ production cross-section is only available for $p_T < 14$ GeV/c. Using the value of

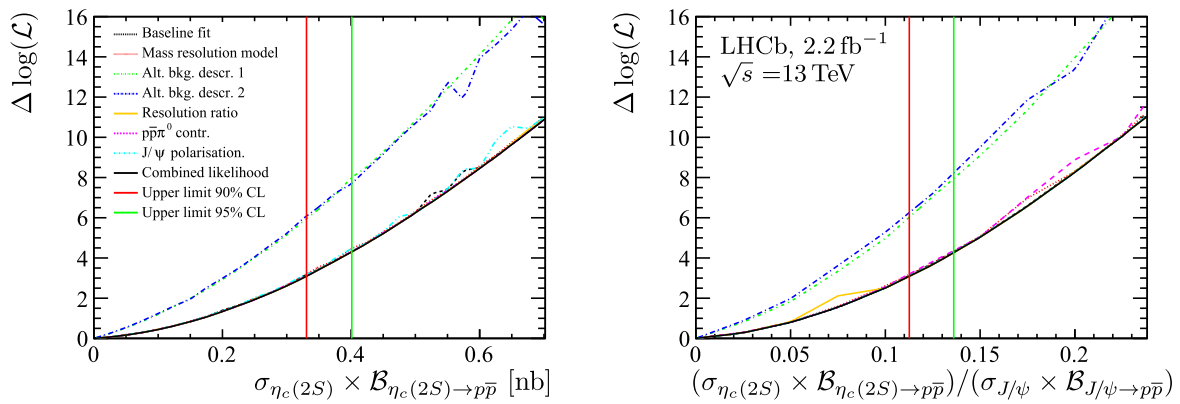


Fig. 2 The log-likelihood profile plots for the (black dashed line) baseline fit and alternative fits including: (red dashed line) alternative mass resolution model, (green and blue dashed lines) alternative models of combinatorial background, (orange dashed line) alternative resolution ratio, (magenta dashed line) alternative contribution from partially reconstructed $J/\psi \rightarrow p\bar{p}\pi^0$ decay, and (cyan dashed line) accounting

for the nonzero J/ψ polarisation. The black solid line represents the log-likelihood profile obtained using the discrete profiling method [34]. The solid red and green lines show Bayesian upper limits on (left) $\eta_c(2S)$ and (right) relative $\eta_c(2S)$ to J/ψ prompt-production cross-section at 90% and 95% CL, respectively

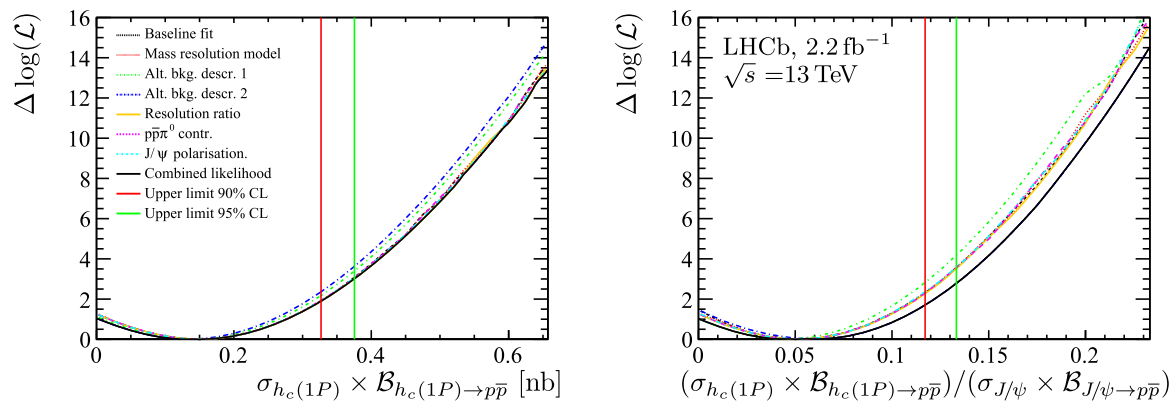


Fig. 3 The log-likelihood profile plots for the (black dashed line) baseline fit and alternative fits including: (red dashed line) alternative mass resolution model, (green and blue dashed lines) alternative models of combinatorial background, (orange dashed line) alternative resolution ratio, (magenta dashed line) alternative contribution from partially reconstructed $J/\psi \rightarrow p\bar{p}\pi^0$ decay, and (cyan dashed line) account-

ing for the nonzero J/ψ polarisation. The black solid line represents the log-likelihood profile obtained using the discrete profiling method [34]. The solid red and green lines show Bayesian upper limits on (left) $h_c(1P)$ and (right) relative $h_c(1P)$ to J/ψ prompt-production cross-section at 90% and 95% CL, respectively

Table 7 Upper limits (UL) at 95% CL for $\eta_c(2S)$ relative to J/ψ and $\eta_c(2S)$ absolute prompt production cross-section, and its comparison with NLO NRQCD theoretical prediction (Refs. [7–10])

p_T [GeV/c]	UL 95% CL	Shao et al. [8]	Gong et al. [9]	Bodwin et al. [10]
	$\sigma_{\eta_c(2S)} \times \mathcal{B}_{\eta_c(2S) \rightarrow p\bar{p}}$ [pb]			
5.0–14.0	< 426	664 ± 297	365 ± 135	855 ± 123
5.0–20.0	< 401	674 ± 304	368 ± 138	870 ± 126
	$(\sigma_{\eta_c(2S)} \times \mathcal{B}_{\eta_c(2S) \rightarrow p\bar{p}}) / (\sigma_{J/\psi} \times \mathcal{B}_{J/\psi \rightarrow p\bar{p}})$			
5.0–14.0, $y < 4.0$	< 0.14	0.48 ± 0.22	0.27 ± 0.10	0.62 ± 0.09
5.0–14.0, $y < 4.5$	< 0.14	0.43 ± 0.19	0.24 ± 0.09	0.55 ± 0.08
5.0–20.0, $y < 4.0$	< 0.14			

$\sigma_{J/\psi}^{5.0 < p_T < 14.0 \text{ GeV}/c, 2.0 < y < 4.0} = 1373 \pm 58 \text{ nb}$ from Ref. [15], the absolute η_c prompt production cross-section is measured to be

$$(\sigma_{\eta_c})^{5.0 < p_T < 14.0 \text{ GeV}/c, 2.0 < y < 4.0} = 1815 \pm 189 \pm 120 \pm 192 \text{ nb},$$

where the last uncertainty also includes the uncertainty on the J/ψ production cross-section.

The relative η_c to J/ψ and absolute η_c prompt production cross-section are shown as a function of the centre-of-mass energy in Fig. 4. In addition, the corresponding J/ψ production cross-section in the same kinematic range from Refs. [14, 15, 36] is shown for comparison.

The relative η_c inclusive branching fraction from b -hadron decays is measured to be

$$\mathcal{B}_{b \rightarrow \eta_c X} / \mathcal{B}_{b \rightarrow J/\psi X} = 0.49 \pm 0.03 \pm 0.02 \pm 0.05.$$

Using the value $\mathcal{B}_{b \rightarrow J/\psi X} = 1.16 \pm 0.10\%$ [11], the absolute value is measured to be

$$\mathcal{B}_{b \rightarrow \eta_c X} = (5.64 \pm 0.31 \pm 0.18 \pm 0.73) \times 10^{-3},$$

where the last uncertainty includes the uncertainty on the $b \rightarrow J/\psi$ inclusive branching fraction.

The relative differential η_c to J/ψ prompt production cross-section is shown in Fig. 5 in bins of p_T and y , and the corresponding values are reported in Tables 11 and 12, respectively. The result of the fit by a linear function to the prompt production cross-section in bins of p_T is overlaid. The slope is found to be $0.118 \pm 0.057 (\text{GeV}/c^{-1})$. A significant slope may indicate the presence of CO contribution to the η_c prompt production cross-section at higher p_T [4].

The absolute differential η_c prompt production cross-sections as a function of p_T and y are shown in Fig. 6. The values are reported in Tables 13 and 14 in bins of p_T and y , respectively.

Relative and absolute prompt p_T -differential production results are compared with the NLO NRQCD predictions for CS and for the sum of CS and CO contributions² and modified NRQCD [37], and shown in Fig. 7. The NRQCD CS model and modified NRQCD show reasonable agreement with data for $p_T > 8 \text{ GeV}/c$, but overestimate data at lower p_T . The sum of the CS and CO contributions overestimates data in the entire p_T range.

6.3 Production of χ_{cJ} mesons in b -hadron decays

The relative yields of the χ_{cJ} states in b -hadron inclusive decays are measured in order to derive the absolute branching ratios of the χ_{cJ} states to $p\bar{p}$.

The relative efficiency-corrected yields of the χ_{cJ} states in b -hadron inclusive decays are measured to be

$$\frac{\mathcal{B}(b \rightarrow \chi_{c1} X) \times \mathcal{B}(\chi_{c1} \rightarrow p\bar{p})}{\mathcal{B}(b \rightarrow \chi_{c0} X) \times \mathcal{B}(\chi_{c0} \rightarrow p\bar{p})} = 0.58 \pm 0.23 \pm 0.02,$$

$$\frac{\mathcal{B}(b \rightarrow \chi_{c2} X) \times \mathcal{B}(\chi_{c2} \rightarrow p\bar{p})}{\mathcal{B}(b \rightarrow \chi_{c0} X) \times \mathcal{B}(\chi_{c0} \rightarrow p\bar{p})} = 0.17 \pm 0.12 \pm 0.01,$$

where the quoted uncertainties are statistical and systematic. The uncertainty in both measurements is dominated by the statistical uncertainty.

Using the known branching ratios of the χ_{cJ} decays to the $p\bar{p}$ final state, $\mathcal{B}_{\chi_{c0} \rightarrow p\bar{p}} = (2.21 \pm 0.8) \times 10^{-4}$, $\mathcal{B}_{\chi_{c1} \rightarrow p\bar{p}} = (7.60 \pm 0.34) \times 10^{-5}$, and $\mathcal{B}_{\chi_{c2} \rightarrow p\bar{p}} = (7.33 \pm 0.33) \times 10^{-5}$ [11], the ratios of the branching fractions of the b -hadron inclusive decays to the χ_{cJ} states are measured to be

$$\frac{\mathcal{B}(b \rightarrow \chi_{c1} X)}{\mathcal{B}(b \rightarrow \chi_{c0} X)} = 1.68 \pm 0.66 \pm 0.05 \pm 0.10,$$

$$\frac{\mathcal{B}(b \rightarrow \chi_{c2} X)}{\mathcal{B}(b \rightarrow \chi_{c0} X)} = 0.50 \pm 0.36 \pm 0.04 \pm 0.03,$$

where the quoted uncertainties are statistical, systematic and from the branching fractions of the χ_{cJ} decays to $p\bar{p}$ final state, respectively.

Precise measurements of the branching ratios of the J/ψ decay to the $p\bar{p}$ final state and the inclusive b -hadron decay to the J/ψ final state enable an improved precision of the measurements for the χ_{c0} and χ_{c1} states. The product of the branching fractions of b -hadron decays to χ_{cJ} and the branching fractions of the $\chi_{cJ} \rightarrow p\bar{p}$ decay mode are determined as

$$\mathcal{B}_{b \rightarrow \chi_{c0} X} \times \mathcal{B}_{\chi_{c0} \rightarrow p\bar{p}} = (6.74 \pm 1.18 \pm 0.18 \pm 0.59) \times 10^{-7},$$

$$\mathcal{B}_{b \rightarrow \chi_{c1} X} \times \mathcal{B}_{\chi_{c1} \rightarrow p\bar{p}} = (3.88 \pm 0.91 \pm 0.11 \pm 0.34) \times 10^{-7},$$

$$\mathcal{B}_{b \rightarrow \chi_{c2} X} \times \mathcal{B}_{\chi_{c2} \rightarrow p\bar{p}} = (1.13 \pm 0.83 \pm 0.03 \pm 0.10) \times 10^{-7}.$$

The quoted uncertainties are statistical, systematic and related to the $\mathcal{B}_{J/\psi \rightarrow p\bar{p}}$, and $\mathcal{B}_{b \rightarrow J/\psi X}$ uncertainties. The computed branching ratios of inclusive b -hadron decays to χ_{cJ} are presented in Table 8.

The values are compared with the previous LHCb measurement of χ_{cJ} production in b -hadron decays [38] and with the world averages [11]. Both LHCb results are in good agreement. The presented measurements of the χ_{c0} and χ_{c1} production in b -hadron decays are the most precise to date.

7 Summary

Using pp collision data corresponding to an integrated luminosity of 2.2 fb^{-1} collected by the LHCb experiment at

² The prediction is provided by H.S. Shao based on Ref. [4] in the kinematic range corresponding to that presented in this analysis.

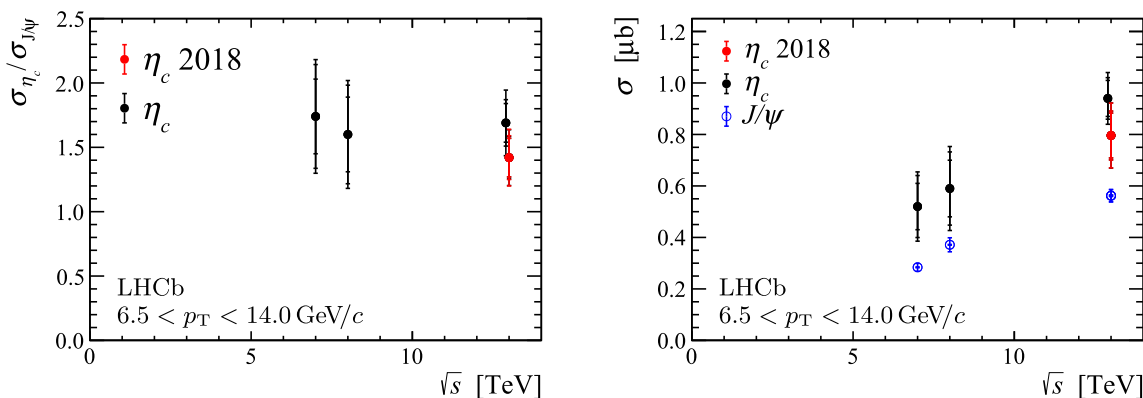


Fig. 4 Left: measured η_c to J/ψ cross-section ratio at different centre-of-mass energies. Right: measured η_c and J/ψ [14, 15, 36] prompt production cross-sections. The red points show the result from the current analysis. The error bars show following uncertainties: statistical, sys-

tematic, and due to the $J/\psi \rightarrow p\bar{p}$ and $\eta_c \rightarrow p\bar{p}$ branching fractions (and J/ψ production cross-section for the absolute production cross-section)

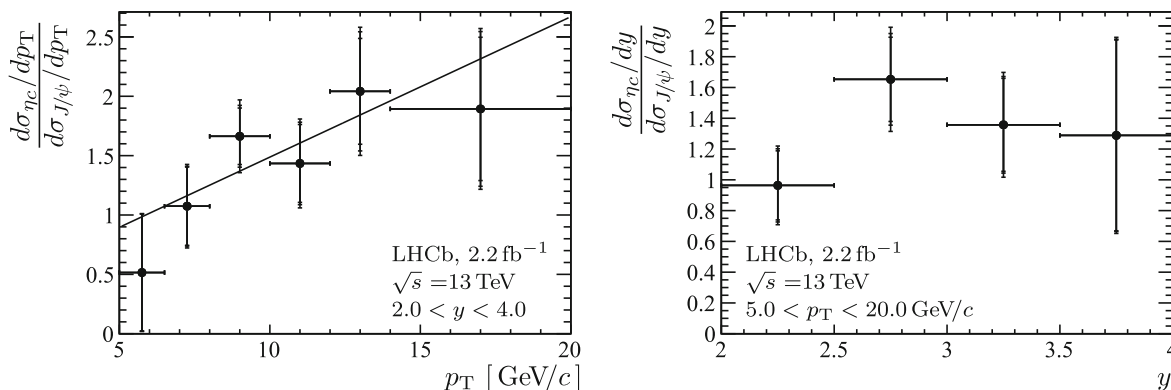


Fig. 5 Measured η_c to J/ψ prompt-production cross-section ratio in intervals of (left) p_T and (right) y . The error bars show following uncertainties: statistical, systematic, and due to the branching fractions

$\mathcal{B}_{J/\psi \rightarrow p\bar{p}}$ and $\mathcal{B}_{\eta_c \rightarrow p\bar{p}}$ uncertainties. The result of the fit with a linear function for p_T -differential cross-section is overlaid

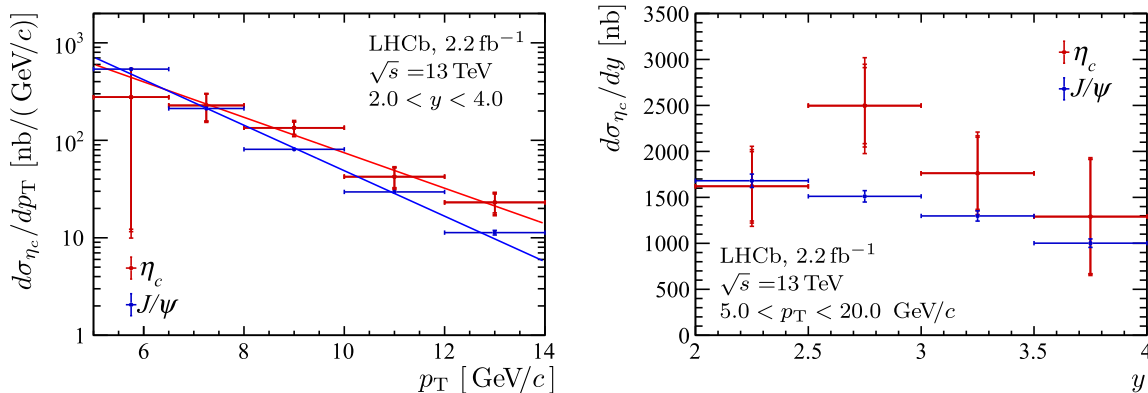


Fig. 6 Measurement of the differential prompt production cross-section of the (red) η_c and (blue) J/ψ mesons [15] in bins of (left) p_T - and (right) y . The error bars show following uncertainties for η_c produc-

tion: statistical, systematic, and the uncertainty due to the $J/\psi \rightarrow p\bar{p}$ and $\eta_c \rightarrow p\bar{p}$ branching fractions and J/ψ production cross-section. The results of the fits with exponential functions are overlaid

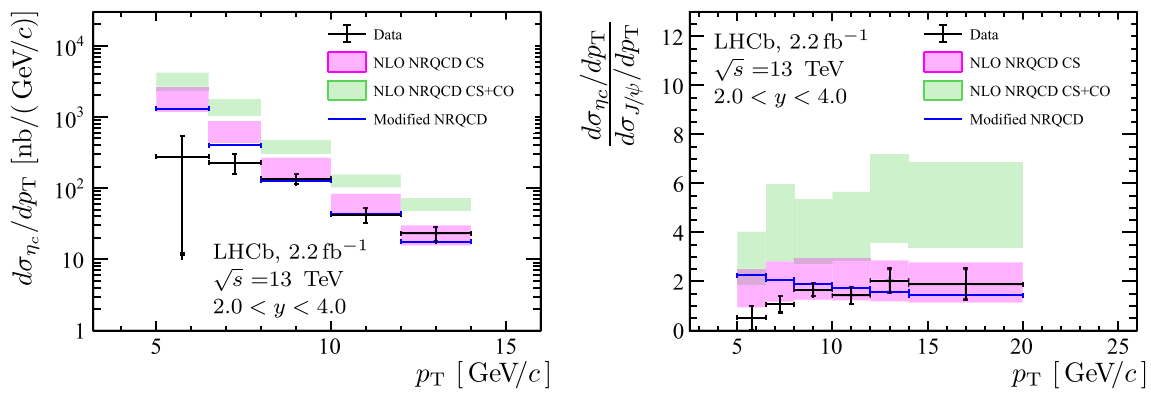


Fig. 7 Measurement of the (left) absolute η_c and (right) relative η_c to J/ψ p_T -differential prompt-production cross-section. Magenta boxes represent NLO NRQCD CS prediction; green boxes show the sum of NLO NRQCD CS and CO predictions. Blue lines represent the modified NRQCD prediction [37]

Table 8 Branching fractions of χ_{cJ} production in inclusive b -hadron decays. The quoted uncertainties are statistical, systematic and the related to the $\mathcal{B}_{\chi_{cJ} \rightarrow p\bar{p}}$, $\mathcal{B}_{J/\psi \rightarrow p\bar{p}}$, and $\mathcal{B}_{b \rightarrow J/\psi X}$ uncertainties. The val-

ues are compared with results from analysis of charmonia production using decays to $\phi\phi$ [38] and the world average values [11]

	$c\bar{c} \rightarrow p\bar{p}$, measured	$c\bar{c} \rightarrow \phi\phi$ [38]	World average [11]
$\mathcal{B}_{b \rightarrow \chi_{c0} X} \times 10^{-3}$	$3.05 \pm 0.54 \pm 0.08 \pm 0.29$	3.02 ± 1.08	15 ± 6
$\mathcal{B}_{b \rightarrow \chi_{c1} X} \times 10^{-3}$	$5.11 \pm 1.20 \pm 0.14 \pm 0.50$	2.76 ± 1.09	14 ± 4
$\mathcal{B}_{b \rightarrow \chi_{c2} X} \times 10^{-3}$	$1.54 \pm 1.13 \pm 0.04 \pm 0.15$	1.15 ± 0.42	6.2 ± 2.9

$\sqrt{s} = 13$ TeV in 2018, the upper limits on the ratio of the $\eta_c(2S)$ and $h_c(1P)$ to J/ψ prompt production cross-section, at 90% (95%) CL, are determined for the first time as

$$\frac{(\sigma_{\eta_c(2S)} \times \mathcal{B}_{\eta_c(2S) \rightarrow p\bar{p}})}{(\sigma_{J/\psi} \times \mathcal{B}_{J/\psi \rightarrow p\bar{p}})} < 0.11 \quad (0.14),$$

$$\frac{(\sigma_{h_c(1P)} \times \mathcal{B}_{h_c(1P) \rightarrow p\bar{p}})}{(\sigma_{J/\psi} \times \mathcal{B}_{J/\psi \rightarrow p\bar{p}})} < 0.12 \quad (0.13),$$

in the kinematic range $5.0 < p_T < 20.0$ GeV/c and $2.0 < y < 4.0$. The upper limits on the $\eta_c(2S)$ and $h_c(1P)$ prompt production cross-sections multiplied by their decay branching fractions to the $p\bar{p}$ final state are determined.

The relative η_c to J/ψ prompt production cross-section is measured in the extended kinematic range compared to the previous analysis, $5.0 < p_T < 20.0$ GeV/c, leading to

$$(\sigma_{\eta_c} / \sigma_{J/\psi})^{5.0 < p_T < 20.0 \text{ GeV/c}, 2.0 < y < 4.0} = 1.32 \pm 0.14 \pm 0.09 \pm 0.13.$$

Henceforth, the first uncertainty is statistical, and the second is systematic. The third uncertainty is due to the uncertainties on the branching fractions $\mathcal{B}_{\eta_c \rightarrow p\bar{p}}$ and $\mathcal{B}_{J/\psi \rightarrow p\bar{p}}$.

The absolute η_c prompt production cross-section is derived using the J/ψ prompt production cross-section measurement at $\sqrt{s} = 13$ TeV [15]. The relative η_c to J/ψ and the absolute

η_c inclusive branching fractions from b -hadron decays are measured, obtaining

$$\mathcal{B}_{b \rightarrow \eta_c X} / \mathcal{B}_{b \rightarrow J/\psi X} = 0.49 \pm 0.03 \pm 0.02 \pm 0.05,$$

$$\mathcal{B}_{b \rightarrow \eta_c X} = (5.64 \pm 0.31 \pm 0.18 \pm 0.73) \times 10^{-3},$$

where the third uncertainty is due to the uncertainties on the branching fractions $\mathcal{B}_{\eta_c \rightarrow p\bar{p}}$ and $\mathcal{B}_{J/\psi \rightarrow p\bar{p}}$ and the uncertainties on the branching fractions $\mathcal{B}_{\eta_c \rightarrow p\bar{p}}$, $\mathcal{B}_{J/\psi \rightarrow p\bar{p}}$ and $\mathcal{B}_{b \rightarrow J/\psi X}$, respectively. The results on η_c production are consistent with the previous LHCb measurement at $\sqrt{s} = 13$ TeV [5]. The η_c prompt production cross-section at low p_T is below the available theoretical expectations and calls for an improved theory description in this range.

New measurements of the branching fractions $\mathcal{B}_{b \rightarrow \chi_{cJ} X} \times \mathcal{B}_{\chi_{cJ} \rightarrow p\bar{p}}$ and $\mathcal{B}_{b \rightarrow \chi_{cJ} X}$ are reported. The inclusive branching fraction results for the χ_{c0} and χ_{c1} mesons,

$$\mathcal{B}_{b \rightarrow \chi_{c0} X} = (3.05 \pm 0.54 \pm 0.08 \pm 0.29) \times 10^{-3},$$

$$\mathcal{B}_{b \rightarrow \chi_{c1} X} = (5.11 \pm 1.20 \pm 0.14 \pm 0.50) \times 10^{-3},$$

are the most precise to date. The third uncertainty here is due to the uncertainties on the branching fractions $\mathcal{B}_{\chi_{c0,1} \rightarrow p\bar{p}}$, $\mathcal{B}_{J/\psi \rightarrow p\bar{p}}$ and $\mathcal{B}_{b \rightarrow J/\psi X}$.

Acknowledgements We thank J.P. Lansberg, H.S. Shao and K. Sridhar for useful discussions and for providing predictions for charmonium production. We express our gratitude to our colleagues in the CERN accelerator departments for the excellent performance of the LHC. We thank the technical and administrative staff at the LHCb institutes. We acknowledge support from CERN and from the national agencies: CAPES, CNPq, FAPERJ and FINEP (Brazil); MOST and NSFC (China); CNRS/IN2P3 (France); BMBF, DFG and MPG (Germany); INFN (Italy); NWO (Netherlands); MNiSW and NCN (Poland); MCID/IFA (Romania); MICIU and AEI (Spain); SNSF and SER (Switzerland); NASU (Ukraine); STFC (United Kingdom); DOE NP and NSF (USA). We acknowledge the computing resources that are provided by CERN, IN2P3 (France), KIT and DESY (Germany), INFN (Italy), SURF (Netherlands), PIC (Spain), GridPP (United Kingdom), CSCS (Switzerland), IFIN-HH (Romania), CBPF (Brazil), and Polish WLCG (Poland). We are indebted to the communities behind the multiple open-source software packages on which we depend. Individual groups or members have received support from ARC and ARDC (Australia); Key Research Program of Frontier Sciences of CAS, CAS PIFI, CAS CCEPP, Fundamental Research Funds for the Central Universities, and Sci. & Tech. Program of Guangzhou (China); Minciencias (Colombia); EPLANET, Marie Skłodowska-Curie Actions, ERC and NextGenerationEU (European Union); A*MIDEX, ANR, IPhU and Labex P2IO, and Région Auvergne-Rhône-Alpes (France); AvH Foundation (Germany); ICSC (Italy); Severo Ochoa and María de Maeztu Units of Excellence, GVA, XuntaGal, GENCAT, InTalent-Inditex and Prog. Atracción Talento CM (Spain); SRC (Sweden); the Leverhulme Trust, the Royal Society and UKRI (United Kingdom).

Data Availability Statement This manuscript has associated data in a data repository. [Author's comment: The LHCb experiment has agreed to the CERN open data policy that is summarised in <https://opendata.cern.ch/docs/about>. In particular, Level 1 data associated with this publication are made available on the CERN document server at <https://cds.cern.ch/record/2905173>. These data contain material related to the paper that allows a reinterpretation of the results in the context of new theoretical models. Level 3 data are also available from the CERN open data portal, but due to the large amount of data, only the Run1 dataset has been made public up to now.]

Code Availability Statement Code/software will be made available on reasonable request. [Author's comment: Software/Code that is associated with this publication and that is publicly available is referenced within the publication content. Specific analysis software/code used to produce the results shown in the publication is preserved within the LHCb collaboration internally and can be provided on reasonable request, provided it doesn't contain information that can be associated with unpublished results.]

Open Access This article is licensed under a Creative Commons Attribution 4.0 International License, which permits use, sharing, adaptation, distribution and reproduction in any medium or format, as long as you give appropriate credit to the original author(s) and the source, provide a link to the Creative Commons licence, and indicate if changes were made. The images or other third party material in this article are included in the article's Creative Commons licence, unless indicated otherwise in a credit line to the material. If material is not included in the article's Creative Commons licence and your intended use is not permitted by statutory regulation or exceeds the permitted use, you will need to obtain permission directly from the copyright holder. To view a copy of this licence, visit <http://creativecommons.org/licenses/by/4.0/>. Funded by SCOAP³.

Appendices

A Tables of the relative uncertainties

The relative uncertainties for p_T - and y -differential prompt production cross-sections are shown in Tables 9 and 10, respectively. The uncertainties are expressed in percent, relative to the central value in each bin. The total systematic uncertainty is calculated as the quadratic sum of the individual sources.

Table 9 Relative uncertainties (in %) on the ratio of prompt cross-sections $\sigma_{\eta_c}/\sigma_{J/\psi}$ in bins of the η_c transverse momentum, p_T . Uncertainties on $\mathcal{B}_{\eta_c \rightarrow p\bar{p}}$ and $\mathcal{B}_{J/\psi \rightarrow p\bar{p}}$ are considered separately and given in the text

	p_T [GeV/c]					
	5.0–6.5	6.5–8.0	8.0–10.0	10.0–12.0	12.0–14.0	14.0–20.0
Statistical uncertainty	95.6	30.7	14.3	22.9	21.8	31.9
Combinatorial background	4.0	3.9	3.8	3.6	3.5	3.2
Contribution from $J/\psi \rightarrow p\bar{p}\pi^0$	0.1	< 0.1	0.1	0.2	0.3	0.5
Resolution p_T -dependence	0.1	< 0.1	0.1	0.3	0.4	0.6
Cross-feed	< 0.1	0.1	0.1	0.1	0.2	0.3
Total uncorrelated systematic	4.0	3.9	3.8	3.6	3.5	3.4
Variation of Γ_{η_c}	1.5	1.1	1.7	1.6	1.7	1.8
Mass resolution model	3.5	2.4	1.6	2.2	1.1	0.6
Polarisation of J/ψ	2.1	1.8	1.6	1.3	1.2	0.9
Total correlated systematic	3.3	3.1	2.9	2.8	2.8	2.6
Total systematic	5.1	4.9	4.8	4.6	4.5	4.3

Table 10 Relative uncertainties (in %) on the ratio of prompt cross-sections $\sigma_{\eta_c}/\sigma_{J/\psi}$ in bins of the η_c rapidity, y . Uncertainties on $\mathcal{B}_{\eta_c \rightarrow p\bar{p}}$ and $\mathcal{B}_{J/\psi \rightarrow p\bar{p}}$ are considered separately and given in the text

	y			
	2.0–2.5	2.5–3.0	3.0–3.5	3.5–4.0
Statistical uncertainty	23.3	16.6	22.3	48.1
Combinatorial background	6.5	5.4	4.3	3.2
Contribution from $J/\psi \rightarrow p\bar{p}\pi^0$	0.4	0.2	< 0.1	0.2
Resolution y -dependence	1.0	0.6	0.3	< 0.1
Cross-feed	0.1	0.1	0.1	0.1
Total uncorrelated systematic	6.6	5.5	4.3	3.2
Variation of Γ_{η_c}	1.0	1.4	1.4	1.4
Mass resolution model	0.1	1.2	0.3	1.7
Polarisation of J/ψ	2.2	1.5	1.2	1.4
Total correlated systematic	3.3	2.9	2.8	2.8
Total systematic	7.4	6.2	5.1	4.3

B Tables of differential production cross-sections

B.1 Relative differential production cross-sections

The relative p_T - and y -differential η_c to J/ψ prompt production cross-sections are shown in Tables 11 and 12. The first uncertainty is statistical, the second is the uncorrelated systematic uncertainty, the third is the systematic uncertainty correlated among bins, and the last one is the uncertainty related to $\mathcal{B}_{J/\psi \rightarrow p\bar{p}}$ and $\mathcal{B}_{\eta_c \rightarrow p\bar{p}}$ branching fractions.

Table 11 Relative p_T -differential η_c prompt production cross-section

p_T [GeV/c]	$d\sigma_{\eta_c}/d\sigma_{J/\psi}$
5.0–6.5	$0.52 \pm 0.49 \pm 0.03 \pm 0.02 \pm 0.05$
6.5–8.0	$1.07 \pm 0.33 \pm 0.06 \pm 0.03 \pm 0.10$
8.0–10.0	$1.66 \pm 0.24 \pm 0.09 \pm 0.05 \pm 0.16$
10.0–12.0	$1.43 \pm 0.33 \pm 0.11 \pm 0.04 \pm 0.14$
12.0–14.0	$2.04 \pm 0.45 \pm 0.22 \pm 0.06 \pm 0.20$
14.0–20.0	$1.89 \pm 0.60 \pm 0.24 \pm 0.05 \pm 0.18$
5.0–14.0	$1.29 \pm 0.15 \pm 0.07 \pm 0.04 \pm 0.13$
6.4–14.0	$1.42 \pm 0.15 \pm 0.05 \pm 0.04 \pm 0.14$
5.0–20.0	$1.32 \pm 0.14 \pm 0.08 \pm 0.04 \pm 0.13$

Table 12 Relative y -differential η_c prompt production cross-section

y	$d\sigma_{\eta_c}/d\sigma_{J/\psi}$
2.0–2.5	$0.96 \pm 0.22 \pm 0.07 \pm 0.03 \pm 0.09$
2.5–3.0	$1.65 \pm 0.27 \pm 0.11 \pm 0.05 \pm 0.16$
3.0–3.5	$1.36 \pm 0.30 \pm 0.08 \pm 0.04 \pm 0.13$
3.5–4.0	$1.29 \pm 0.62 \pm 0.07 \pm 0.04 \pm 0.13$

B.2 Absolute differential production cross-sections

The absolute p_T - and y -differential η_c prompt production cross-sections are shown in Tables 13 and 14. The first uncertainty is statistical, the second is the uncorrelated systematic uncertainty, the third is the systematic uncertainty correlated among bins, and the last one is the uncertainty related to $\mathcal{B}_{J/\psi \rightarrow p\bar{p}}$ and $\mathcal{B}_{\eta_c \rightarrow p\bar{p}}$ branching fractions and the J/ψ production cross-section.

Table 13 Absolute p_T -differential η_c prompt production cross-section

p_T [GeV/ c]	$d\sigma_{\eta_c}/dp_T$ [nb/GeV/ c]
5.0–6.5	$277.0 \pm 264.8 \pm 16.9 \pm 9.0 \pm 29.4$
6.5–8.0	$227.8 \pm 69.8 \pm 12.1 \pm 7.0 \pm 24.2$
8.0–10.0	$134.5 \pm 19.2 \pm 7.6 \pm 3.9 \pm 14.3$
10.0–12.0	$42.4 \pm 9.7 \pm 3.2 \pm 1.2 \pm 4.6$
12.0–14.0	$23.1 \pm 5.0 \pm 2.5 \pm 0.6 \pm 2.6$
6.5–14.0	$796.4 \pm 86.6 \pm 30.8 \pm 21.4 \pm 84.4$
5.0–14.0	$1772.8 \pm 205.4 \pm 97.6 \pm 49.0 \pm 187.9$

Table 14 Absolute y -differential η_c prompt production cross-section

y	$d\sigma_{\eta_c}/dy$ [nb]
2.0–2.5	$1620 \pm 377 \pm 121 \pm 53 \pm 172$
2.5–3.0	$2498 \pm 414 \pm 162 \pm 73 \pm 264$
3.0–3.5	$1762 \pm 392 \pm 99 \pm 49 \pm 188$
3.5–4.0	$1291 \pm 621 \pm 69 \pm 37 \pm 139$

References

- J.-P. Lansberg, New observables in inclusive production of quarkonia. *Phys. Rep.* **889**, 1 (2020). <https://doi.org/10.1016/j.physrep.2020.08.007>. arXiv:1903.09185
- M. Butenschoen, Z.-G. He, B.A. Kniehl, η_c production at the LHC challenges nonrelativistic-QCD factorization. *Phys. Rev. Lett.* **114**, 092004 (2015). <https://doi.org/10.1103/PhysRevLett.114.092004>. arXiv:1411.5287
- LHCb Collaboration, R. Aaij et al., Measurement of the $\eta_c(1S)$ production cross-section in proton-proton collisions via the decay $\eta_c(1S) \rightarrow p\bar{p}$. *Eur. Phys. J. C* **75**, 311 (2015). <https://doi.org/10.1140/epjc/s10052-015-3502-x>. arXiv:1409.3612
- H. Han et al., η_c production at LHC and indications on the understanding of J/ψ production. *Phys. Rev. Lett.* **114**, 092005 (2015). <https://doi.org/10.1103/PhysRevLett.114.092005>. arXiv:1411.7350
- LHCb Collaboration, R. Aaij et al., Measurement of the $\eta_c(1S)$ production cross-section in pp collisions at $\sqrt{s} = 13$ TeV. *Eur. Phys. J. C* **80**, 191 (2020). <https://doi.org/10.1140/epjc/s10052-020-7733-0>. arXiv:1911.03326
- J.-P. Lansberg, M.A. Ozelik, Curing the unphysical behaviour of NLO quarkonium production at the LHC and its relevance to constrain the gluon PDF at low scales. *Eur. Phys. J. C* **81**, 497 (2021). <https://doi.org/10.1140/epjc/s10052-021-09258-7>. arXiv:2012.00702
- J.-P. Lansberg, H.-S. Shao, H.-F. Zhang, η_c' Hadroproduction at next-to-leading order and its relevance to ψ' production. arXiv:1711.00265
- H.S. Shao et al., Yields and polarizations of prompt J/ψ and $\psi(2S)$ production in hadronic collisions. *JHEP* **05**, 103 (2015). [https://doi.org/10.1007/JHEP05\(2015\)103](https://doi.org/10.1007/JHEP05(2015)103). arXiv:1411.3300
- B. Gong, L.-P. Wan, J.-X. Wang, H.-F. Zhang, Polarization for prompt J/ψ and $\psi(2S)$ production at the Tevatron and LHC. *Phys. Rev. Lett.* **110**, 042002 (2013). <https://doi.org/10.1103/PhysRevLett.110.042002>. arXiv:1205.6682
- G.T. Bodwin et al., Fragmentation contributions to hadroproduction of prompt J/ψ , χ_{cJ} , and $\psi(2S)$ states. *Phys. Rev. D* **93**, 034041 (2016). <https://doi.org/10.1103/PhysRevD.93.034041>. arXiv:1509.07904
- Particle Data Group, R.L. Workman et al., Review of particle physics. *Prog. Theor. Exp. Phys.* **2022**, 083C01 (2022). <https://doi.org/10.1093/ptep/ptac097>
- LHCb Collaboration, R. Aaij et al., Measurement of J/ψ production in pp collisions at $\sqrt{s} = 2.76$ TeV. *JHEP* **02**, 041 (2013). [https://doi.org/10.1007/JHEP02\(2013\)041](https://doi.org/10.1007/JHEP02(2013)041). arXiv:1212.1045
- LHCb Collaboration, R. Aaij et al., Measurement of J/ψ production in pp collisions at $\sqrt{s} = 7$ TeV. *Eur. Phys. J. C* **71**, 1645 (2011). <https://doi.org/10.1140/epjc/s10052-011-1645-y>. arXiv:1103.0423
- LHCb Collaboration, R. Aaij et al., Production of J/ψ and Υ mesons in pp collisions at $\sqrt{s} = 8$ TeV. *JHEP* **06**, 064 (2013). [https://doi.org/10.1007/JHEP06\(2013\)064](https://doi.org/10.1007/JHEP06(2013)064). arXiv:1304.6977
- LHCb Collaboration, R. Aaij et al., Measurement of forward J/ψ production cross-sections in pp collisions at $\sqrt{s} = 13$ TeV. *JHEP* **10**, 172 (2015) [Erratum *ibid.* **05**, (2017) 063]. [https://doi.org/10.1007/JHEP10\(2015\)172](https://doi.org/10.1007/JHEP10(2015)172). [https://doi.org/10.1007/JHEP05\(2017\)063](https://doi.org/10.1007/JHEP05(2017)063). arXiv:1509.00771
- LHCb Collaboration, R. Aaij et al., Measurement of $\psi(2S)$ meson production in pp collisions at $\sqrt{s} = 7$ TeV. *Eur. Phys. J. C* **72**, 2100 (2012). [Erratum <https://doi.org/10.1140/epjc/s10052-012-2100-4> *ibid.* **C80** (2020) 49]. <https://doi.org/10.1140/epjc/s10052-012-2100-4>. arXiv:1204.1258
- LHCb Collaboration, R. Aaij et al., Measurement of $\psi(2S)$ production cross-sections in proton-proton collisions at $\sqrt{s} = 7$ and 13 TeV. *Eur. Phys. J. C* **80**, 185 (2020). <https://doi.org/10.1140/epjc/s10052-020-7638-y>. arXiv:1908.03099
- LHCb Collaboration, R. Aaij et al., Measurement of the cross-section ratio $\sigma(\chi_{c2})/\sigma(\chi_{c1})$ for prompt χ_c production at $\sqrt{s} = 7$ TeV. *Phys. Lett. B* **714**, 215 (2012). <https://doi.org/10.1016/j.physletb.2012.06.077>. arXiv:1202.1080
- LHCb Collaboration, R. Aaij et al., Measurement of the relative rate of prompt χ_{c0} , χ_{c1} and χ_{c2} production at $\sqrt{s} = 7$ TeV. *JHEP* **10**, 115 (2013). [https://doi.org/10.1007/JHEP10\(2013\)115](https://doi.org/10.1007/JHEP10(2013)115). arXiv:1307.4285

20. LHCb Collaboration, A.A. Alves Jr. et al., The LHCb detector at the LHC. *JINST* **3**, S08005 (2008). <https://doi.org/10.1088/1748-0221/3/08/S08005>
21. LHCb Collaboration, R. Aaij et al., LHCb detector performance. *Int. J. Mod. Phys. A* **30**, 1530022 (2015). <https://doi.org/10.1142/S0217751X15300227>. arXiv:1412.6352
22. G. Dujany, B. Storaci, Real-time alignment and calibration of the LHCb Detector in Run II. *J. Phys. Conf. Ser.* **664**, 082010 (2015). <https://doi.org/10.1088/1742-6596/664/8/082010>
23. R. Aaij et al., The LHCb trigger and its performance in 2011. *JINST* **8**, P04022 (2013). <https://doi.org/10.1088/1748-0221/8/04/P04022>. arXiv:1211.3055
24. R. Aaij et al., Tesla: an application for real-time data analysis in high energy physics. *Comput. Phys. Commun.* **208**, 35 (2016). <https://doi.org/10.1016/j.cpc.2016.07.022>. arXiv:1604.05596
25. LHCb Collaboration, R. Aaij et al., Momentum scale calibration of the LHCb spectrometer. *JINST* **19**, P02008 (2024). <https://doi.org/10.1088/1748-0221/19/02/P02008>. arXiv:2312.01772
26. T. Sjöstrand, S. Mrenna, P. Skands, PYTHIA 6.4 physics and manual. *JHEP* **05**, 026 (2006). <https://doi.org/10.1088/1126-6708/2006/05/026>. arXiv:hep-ph/0603175
27. T. Sjöstrand, S. Mrenna, P. Skands, A brief introduction to PYTHIA 8.1. *Comput. Phys. Commun.* **178**, 852 (2008). <https://doi.org/10.1016/j.cpc.2008.01.036>. arXiv:0710.3820
28. I. Belyaev et al., Handling of the generation of primary events in Gauss, the LHCb simulation framework. *J. Phys. Conf. Ser.* **331**, 032047 (2011). <https://doi.org/10.1088/1742-6596/331/3/032047>
29. D.J. Lange, The EvtGen particle decay simulation package. *Nucl. Instrum. Methods A* **462**, 152 (2001). [https://doi.org/10.1016/S0168-9002\(01\)00089-4](https://doi.org/10.1016/S0168-9002(01)00089-4)
30. P. Golonka, Z. Was, PHOTOS Monte Carlo: a precision tool for QED corrections in Z and W decays. *Eur. Phys. J. C* **45**, 97 (2006). <https://doi.org/10.1140/epjc/s2005-02396-4>. arXiv:hep-ph/0506026
31. Geant4 Collaboration, S. Agostinelli et al., Geant4: a simulation toolkit. *Nucl. Instrum. Methods A* **506**, 250 (2003). [https://doi.org/10.1016/S0168-9002\(03\)01368-8](https://doi.org/10.1016/S0168-9002(03)01368-8)
32. Geant4 Collaboration, J. Allison et al., Geant4 developments and applications. *IEEE Trans. Nucl. Sci.* **53**, 270 (2006). <https://doi.org/10.1109/TNS.2006.869826>
33. R. Aaij et al., Selection and processing of calibration samples to measure the particle identification performance of the LHCb experiment in Run 2. *Eur. Phys. J. Tech. Instrum.* **6**, 1 (2019). <https://doi.org/10.1140/epjti/s40485-019-0050-z>. arXiv:1803.00824
34. P.D. Dauncey, M. Kenzie, N. Wardle, G.J. Davies, Handling uncertainties in background shapes: the discrete profiling method. *JINST* **10**, P04015 (2015). <https://doi.org/10.1088/1748-0221/10/04/P04015>. arXiv:1408.6865
35. G. D'Agostini, Bayesian inference in processing experimental data: principles and basic applications. *Rep. Prog. Phys.* **66**, 1383 (2003). <https://doi.org/10.1088/0034-4885/66/9/201>. arXiv:physics/0304102
36. LHCb Collaboration, R. Aaij et al., Measurement of J/ψ polarization in pp collisions at $\sqrt{s} = 7$ TeV. *Eur. Phys. J. C* **73**, 2631 (2013). <https://doi.org/10.1140/epjc/s10052-013-2631-3>. arXiv:1307.6379
37. S.S. Biswal, S.S. Mishra, K. Sridhar, Resolution of the LHCb η_c anomaly. *JHEP* **05**, 120 (2023). [https://doi.org/10.1007/JHEP05\(2023\)120](https://doi.org/10.1007/JHEP05(2023)120). arXiv:2301.03158
38. LLHCb Collaboration, R. Aaij et al., Study of charmonium production in b -hadron decays and first evidence for the decay $B_s^0 \rightarrow \phi\phi$. *Eur. Phys. J. C* **77**, 609 (2017). <https://doi.org/10.1140/epjc/s10052-017-5151-8>. arXiv:1706.07013

LHCb Collaboration

R. Aaij³⁶, A.S.W. Abdelmotteleb⁵⁵, C. Abellan Beteta⁴⁹, F. Abudinén⁵⁵, T. Ackernley⁵⁹, A. A. Adefisoye⁶⁷, B. Adeva⁴⁵, M. Adinolfi⁵³, P. Adlarson⁷⁹, C. Agapopoulou¹³, C.A. Aidala⁸⁰, Z. Ajaltouni¹¹, S. Akar⁶⁴, K. Akiba³⁶, P. Albicocco²⁶, J. Albrecht¹⁸, F. Alessio⁴⁷, M. Alexander⁵⁸, Z. Aliouche⁶¹, P. Alvarez Cartelle⁵⁴, R. Amalric¹⁵, S. Amato³, J.L. Amey⁵³, Y. Amhis^{13,47}, L. An⁶, L. Anderlini²⁵, M. Andersson⁴⁹, A. Andreianov⁴², P. Andreola⁴⁹, M. Andreotti²⁴, D. Andreou⁶⁷, A. Anelli^{29,p}, D. Ao⁷, F. Archilli^{35,v}, M. Argenton²⁴, S. Argüedas Cuendis⁹, A. Artamonov⁴², M. Artuso⁶⁷, E. Aslanides¹², M. Atzeni⁶³, B. Audurier¹⁴, D. Bacher⁶², I. Bachiller Perea¹⁰, S. Bachmann²⁰, M. Bachmayer⁴⁸, J.J. Back⁵⁵, P. Baladron Rodriguez⁴⁵, V. Balagura¹⁴, W. Baldini²⁴, H. Bao⁷, J. Baptista de Souza Leite⁵⁹, M. Barbeti^{25,m}, I. R. Barbosa⁶⁸, R.J. Barlow⁶¹, M. Barnyakov²³, S. Barsuk¹³, W. Barter⁵⁷, M. Bartolini⁵⁴, J. Bartz⁶⁷, F. Baryshnikov⁴², J.M. Basels¹⁶, G. Bassi³³, B. Batsukh⁵, A. Bay⁴⁸, A. Beck⁵⁵, M. Becker¹⁸, F. Bedeschi³³, I.B. Bediaga², S. Belin⁴⁵, V. Bellec⁴⁹, K. Belous⁴², I. Belov²⁷, I. Belyaev³⁴, G. Benane¹², G. Bencivenni²⁶, E. Ben-Haim¹⁵, A. Berezhnoy⁴², R. Bernet⁴⁹, S. Bernet Andres⁴³, A. Bertolin³¹, C. Betancourt⁴⁹, F. Betti⁵⁷, J. Bex⁵⁴, Ia. Bezshyiko⁴⁹, J. Bhom³⁹, M.S. Bieker¹⁸, N.V. Biesuz²⁴, P. Billoir¹⁵, A. Biolchini³⁶, M. Birch⁶⁰, F.C.R. Bishop¹⁰, A. Bitadze⁶¹, A. Bizzeti, T. Blake⁵⁵, F. Blanc⁴⁸, J.E. Blank¹⁸, S. Blusk⁶⁷, V. Bocharnikov⁴², J.A. Boelhauve¹⁸, O. Boente Garcia¹⁴, T. Boettcher⁶⁴, A. Bohare⁵⁷, A. Boldyrev⁴², C.S. Bolognani⁷⁶, R. Bolzonella^{24,1}, N. Bondar⁴², F. Borgato^{31,q,47}, S. Borghi⁶¹, M. Borsato^{29,p}, J.T. Borsuk³⁹, S.A. Bouchiba⁴⁸, T.J.V. Bowcock⁵⁹, A. Boyer⁴⁷, C. Bozzi²⁴, M. J. Bradley⁶⁰, A. Brea Rodriguez⁴⁸, N. Breer¹⁸, J. Brodzicka³⁹, A. Brossa Gonzalo⁴⁵, J. Brown⁵⁹, D. Brundu³⁰, E. Buchanan⁵⁷, A. Buonaura⁴⁹, L. Buonincontri^{31,q}, A.T. Burke⁶¹, C. Burr⁴⁷, A. Butkevich⁴²,

J.S. Butter⁵⁴, J. Buytaert⁴⁷, W. Byczynski⁴⁷, S. Cadeddu³⁰, H. Cai⁷², R. Calabrese^{24,1}, S. Calderon Ramirez⁹, L. Calefice⁴⁴, S. Cali²⁶, M. Calvi^{29,p}, M. Calvo Gomez⁴³, P. Camargo Magalhaes^{2,z}, J. I. Cambon Bouzas⁴⁵, P. Campana²⁶, D.H. Campora Perez⁷⁶, A.F. Campoverde Quezada⁷, S. Capelli²⁹, L. Capriotti²⁴, R. Caravaca-Mora⁹, A. Carbone^{23,j}, L. Carcedo Salgado⁴⁵, R. Cardinale^{27,n}, A. Cardini³⁰, P. Carniti^{29,p}, L. Carus²⁰, A. Casais Vidal⁶³, R. Caspary²⁰, G. Casse⁵⁹, J. Castro Godinez⁹, M. Cattaneo⁴⁷, G. Cavallero^{24,47}, V. Cavallini^{24,1}, S. Celani²⁰, D. Cervenkov⁶², S. Cesare^{28,o}, A.J. Chadwick⁵⁹, I. Chahrour⁸⁰, M. Charles¹⁵, Ph. Charpentier⁴⁷, C.A. Chavez Barajas⁵⁹, M. Chefdeville¹⁰, C. Chen¹², S. Chen⁵, Z. Chen⁷, A. Chernov³⁹, S. Chernyshenko⁵¹, V. Chobanova⁷⁸, S. Cholak⁴⁸, M. Chruszcz³⁹, A. Chubykin⁴², V. Chulikov⁴², P. Ciambrone²⁶, X. Cid Vidal⁴⁵, G. Ciezarek⁴⁷, P. Cifra⁴⁷, P.E.L. Clarke⁵⁷, M. Clemencic⁴⁷, H.V. Cliff⁵⁴, J. Closier⁴⁷, C. Cocha Toapaxi²⁰, V. Coco⁴⁷, J. Cogan¹², E. Cogneras¹¹, L. Cojocariu⁴¹, P. Collins⁴⁷, T. Colombo⁴⁷, A. Comerma-Montells⁴⁴, L. Congedo²², A. Contu³⁰, N. Cooke⁵⁸, I. Corredoira⁴⁵, A. Correia¹⁵, G. Corti⁴⁷, J. J. Cottee Meldrum⁵³, B. Couturier⁴⁷, D.C. Craik⁴⁹, M. Cruz Torres^{2,g}, E. Curras Rivera⁴⁸, R. Currie⁵⁷, C.L. Da Silva⁶⁶, S. Dadabae⁴², L. Dai⁶⁹, X. Dai⁶, E. Dall'Occo¹⁸, J. Dalseno⁴⁵, C. D'Ambrosio⁴⁷, J. Daniel¹¹, A. Danilina⁴², P. d'Argent²², A. Davidson⁵⁵, J.E. Davies⁶¹, A. Davis⁶¹, O. De Aguiar Francisco⁶¹, C. De Angelis^{30,k}, F. De Benedetti⁴⁷, J. de Boer³⁶, K. De Bruyn⁷⁵, S. De Capua⁶¹, M. De Cian^{20,47}, U. De Freitas Carneiro Da Graca^{2,b}, E. De Lucia²⁶, J.M. De Miranda², L. De Paula³, M. De Serio^{22,h}, P. De Simone²⁶, F. De Vellis¹⁸, J.A. de Vries⁷⁶, F. Debernardis²², D. Decamp¹⁰, V. Dedu¹², L. Del Buono¹⁵, B. Delaney⁶³, H.-P. Dembinski¹⁸, J. Deng⁸, V. Denysenko⁴⁹, O. Deschamps¹¹, F. Dettori^{30,k}, B. Dey⁷⁴, P. Di Nezza²⁶, I. Diachkov⁴², S. Didenko⁴², S. Ding⁶⁷, L. Dittmann²⁰, V. Dobishuk⁵¹, A. D. Docheva⁵⁸, C. Dong⁴, A.M. Donohoe²¹, F. Dordei³⁰, A.C. dos Reis², A. D. Dowling⁶⁷, W. Duan⁷⁰, P. Duda⁷⁷, M.W. Dudek³⁹, L. Dufour⁴⁷, V. Duk³², P. Durante⁴⁷, M. M. Duras⁷⁷, J.M. Durham⁶⁶, O. D. Durmus⁷⁴, A. Dziurda³⁹, A. Dzyuba⁴², S. Easo⁵⁶, E. Eckstein¹⁷, U. Egede¹, A. Egorychev⁴², V. Egorychev⁴², S. Eisenhardt⁵⁷, E. Ejopu⁶¹, L. Eklund⁷⁹, M. Elashri⁶⁴, J. Ellbracht¹⁸, S. Ely⁶⁰, A. Ene⁴¹, E. Epple⁶⁴, J. Eschle⁶⁷, S. Esen²⁰, T. Evans⁶¹, F. Fabiano^{30,k,47}, L.N. Falcao², Y. Fan⁷, B. Fang⁷², L. Fantini^{32,r}, M. Faria⁴⁸, K. Farmer⁵⁷, D. Fazzini^{29,p}, L. Felkowski⁷⁷, M. Feng^{5,7}, M. Feo^{18,47}, M. Fernandez Gomez⁴⁵, A.D. Ferez⁶⁵, F. Ferrari²³, F. Ferreira Rodrigues³, M. Ferrillo⁴⁹, M. Ferro-Luzzi⁴⁷, S. Filippov⁴², R.A. Fini²², M. Fiorini^{24,1}, K.M. Fischer⁶², D.S. Fitzgerald⁸⁰, C. Fitzpatrick⁶¹, F. Fleuret¹⁴, M. Fontana²³, L. F. Foreman⁶¹, R. Forty⁴⁷, D. Foulds-Holt⁵⁴, M. Franco Sevilla⁶⁵, M. Frank⁴⁷, E. Franzoso^{24,1}, G. Frau²⁰, C. Frei⁴⁷, D.A. Friday⁶¹, J. Fu⁷, Q. Fuehring¹⁸, Y. Fujii¹, T. Fulghesu¹⁵, E. Gabriel³⁶, G. Galati²², M.D. Galati³⁶, A. Gallas Torreira⁴⁵, D. Galli^{23,j}, S. Gambetta⁵⁷, M. Gandelman³, P. Gandini²⁸, B. Ganie⁶¹, H. Gao⁷, R. Gao⁶², Y. Gao⁸, Y. Gao⁶, Y. Gao⁸, M. Garau^{30,k}, L.M. Garcia Martin⁴⁸, P. Garcia Moreno⁴⁴, J. Garcia Pardiñas⁴⁷, K. G. Garg⁸, L. Garrido⁴⁴, C. Gaspar⁴⁷, R.E. Geertsema³⁶, L.L. Gerken¹⁸, E. Gersabeck⁶¹, M. Gersabeck⁶¹, T. Gershon⁵⁵, Z. Ghorbanimoghaddam⁵³, L. Giambastiani^{31,q}, F. I. Giasemis^{15,e}, V. Gibson⁵⁴, H.K. Giemza⁴⁰, A.L. Gilman⁶², M. Giovannetti²⁶, A. Gioventù⁴⁴, P. Gironella Gironell⁴⁴, C. Giugliano^{24,1}, M.A. Giza³⁹, E.L. Gkoukousis⁶⁰, F.C. Glaser^{13,20}, V.V. Gligorov^{15,47}, C. Göbel⁶⁸, E. Golobardes⁴³, D. Golubkov⁴², A. Golutvin^{42,47,60}, A. Gomes^{2,a}†, S. Gomez Fernandez⁴⁴, F. Goncalves Abrantes⁶², M. Goncerz³⁹, G. Gong⁴, J. A. Gooding¹⁸, I.V. Gorelov⁴², C. Gotti²⁹, J.P. Grabowski¹⁷, L.A. Granado Cardoso⁴⁷, E. Graugés⁴⁴, E. Graverini^{48,t}, L. Grazzette⁵⁵, G. Graziani, A. T. Grecu⁴¹, L.M. Greeven³⁶, N.A. Grieser⁶⁴, L. Grillo⁵⁸, S. Gromov⁴², C. Gu¹⁴, M. Guarise²⁴, M. Guittiere¹³, V. Guliaeva⁴², P. A. Günther²⁰, A.-K. Guseinov⁴⁸, E. Gushchin⁴², Y. Guz^{6,42,47}, T. Gys⁴⁷, K. Habermann¹⁷, T. Hadavizadeh¹, C. Hadjivasiliou⁶⁵, G. Haefeli⁴⁸, C. Haen⁴⁷, J. Haimberger⁴⁷, M. Hajheidari⁴⁷, M.M. Halvorsen⁴⁷, P.M. Hamilton⁶⁵, J. Hammerich⁵⁹, Q. Han⁸, X. Han²⁰, S. Hansmann-Menzemer²⁰, L. Hao⁷, N. Harnew⁶², M. Hartmann¹³, J. He^{7,c}, F. Hemmer⁴⁷, C. Henderson⁶⁴, R.D.L. Henderson^{1,55}, A.M. Hennequin⁴⁷, K. Hennessy⁵⁹, L. Henry⁴⁸, J. Herd⁶⁰, P. Herrero Gascon²⁰, J. Heuel¹⁶, A. Hicheur³, G. Hijano Mendizabal⁴⁹, D. Hill⁴⁸, S.E. Hollitt¹⁸, J. Horswill⁶¹, R. Hou⁸, Y. Hou¹¹, N. Howarth⁵⁹, J. Hu²⁰, J. Hu⁷⁰, W. Hu⁶, X. Hu⁴, W. Huang⁷, W. Hulsbergen³⁶, R.J. Hunter⁵⁵, M. Hushchyn⁴², D. Hutchcroft⁵⁹, D. Ilin⁴², P. Ilten⁶⁴, A. Inglessi⁴², A. Injukhin⁴², A. Ishteev⁴², K. Ivshin⁴², R. Jacobsson⁴⁷, H. Jage¹⁶, S.J. Jaimes Elles^{46,73}, S. Jakobsen⁴⁷, E. Jans³⁶, B.K. Jashal⁴⁶, A. Jawahery^{47,65}, V. Jevtic¹⁸, E. Jiang⁶⁵, X. Jiang^{5,7}, Y. Jiang⁷, Y. J. Jiang⁶, M. John⁶², D. Johnson⁵², C.R. Jones⁵⁴, T.P. Jones⁵⁵, S. Joshi⁴⁰, B. Jost⁴⁷, N. Jurik⁴⁷, I. Juszczak³⁹, D. Kaminaris⁴⁸, S. Kandybei⁵⁰, Y. Kang⁴, C. Kar¹¹, M. Karacson⁴⁷, D. Karpenkov⁴², A. Kauniskangas⁴⁸, J.W. Kautz⁶⁴, F. Keizer⁴⁷, M. Kenzie⁵⁴, T. Ketel³⁶, B. Khanji⁶⁷, A. Kharisova⁴², S. Kholodenko^{33,47}, G. Khreich¹³, T. Kim¹⁶, V.S. Kirsebom^{29,p}, O. Kitouni⁶³, S. Klaver³⁷, N. Kleijne^{33,s}, K. Klimaszewski⁴⁰,

M.R. Kmiec⁴⁰, S. Koliiev⁵¹, L. Kolk¹⁸, A. Konoplyannikov⁴², P. Kopciwicz^{38,47}, P. Koppenburg³⁶, M. Korolev⁴², I. Kostiuk³⁶, O. Kot⁵¹, S. Kotriakhova, A. Kozachuk⁴², P. Kravchenko⁴², L. Kravchuk⁴², M. Kreps⁵⁵, P. Krokovny⁴², W. Krupa⁶⁷, W. Krzemien⁴⁰, O. K. Kshyvanskiy⁵¹, J. Kubat²⁰, S. Kubis⁷⁷, M. Kucharczyk³⁹, V. Kudryavtsev⁴², E. Kulikova⁴², A. Kupsc⁷⁹, B. K. Kutsenko¹², D. Lacarrere⁴⁷, A. Lai³⁰, A. Lampis³⁰, D. Lancierini⁵⁴, C. Landesa Gomez⁴⁵, J.J. Lane¹, R. Lane⁵³, C. Langenbruch²⁰, J. Langer¹⁸, O. Lantwin⁴², T. Latham⁵⁵, F. Lazzari^{33,1}, C. Lazzeroni⁵², R. Le Gac¹², R. Lefèvre¹¹, A. Leflat⁴², S. Legotin⁴², M. Lehuraux⁵⁵, E. Lemos Cid⁴⁷, O. Leroy¹², T. Lesiak³⁹, B. Leverington²⁰, A. Li⁴, H. Li⁷⁰, K. Li⁸, L. Li⁶¹, P. Li⁴⁷, P.-R. Li⁷¹, Q. Li^{5,7}, S. Li⁸, T. Li^{5,4}, T. Li⁷⁰, Y. Li⁸, Y. Li⁵, Z. Lian⁴, X. Liang⁶⁷, S. Libralon⁴⁶, C. Lin⁷, T. Lin⁵⁶, R. Lindner⁴⁷, V. Lisovskyi⁴⁸, R. Litvinov³⁰, F. L. Liu¹, G. Liu⁷⁰, K. Liu⁷¹, S. Liu^{5,7}, Y. Liu⁵⁷, Y. Liu⁷¹, Y. L. Liu⁶⁰, A. Lobo Salvia⁴⁴, A. Loi³⁰, J. Lomba Castro⁴⁵, T. Long⁵⁴, J.H. Lopes³, A. Lopez Huertas⁴⁴, S. López Soliño⁴⁵, C. Lucarelli^{25,m}, D. Lucchesi^{31,q}, M. Lucio Martinez⁷⁶, V. Lukashenko^{36,51}, Y. Luo⁶, A. Lupato³¹, E. Luppi^{24,1}, K. Lynch²¹, X.-R. Lyu⁷, G. M. Ma⁴, R. Ma⁷, S. Maccolini¹⁸, F. Macheferf¹³, F. Maciuc⁴¹, B. Mack⁶⁷, I. Mackay⁶², L. M. Mackey⁶⁷, L.R. Madhan Mohan⁵⁴, M. M. Madurai⁵², A. Maevskiy⁴², D. Magdalinski³⁶, D. Maisuzenko⁴², M. W. Majewski³⁸, J.J. Malczewski³⁹, S. Malde⁶², L. Malentacca⁴⁷, A. Malinin⁴², T. Maltsev⁴², G. Manca^{30,k}, G. Mancinelli¹², C. Mancuso^{13,28,o}, R. Manera Escalero⁴⁴, D. Manuzzi²³, D. Marangotto^{28,o}, J.F. Marchand¹⁰, R. Marchevski⁴⁸, U. Marconi²³, S. Mariani⁴⁷, C. Marin Benito⁴⁴, J. Marks²⁰, A.M. Marshall⁵³, G. Martelli^{32,r}, G. Martellotti³⁴, L. Martinazzoli⁴⁷, M. Martinelli^{29,p}, D. Martinez Santos⁴⁵, F. Martinez Vidal⁴⁶, A. Massafferri², R. Matev⁴⁷, A. Mathad⁴⁷, V. Matiunin⁴², C. Matteuzzi⁶⁷, K.R. Mattioli¹⁴, A. Mauri⁶⁰, E. Maurice¹⁴, J. Mauricio⁴⁴, P. Mayencourt⁴⁸, M. Mazurek⁴⁰, M. McCann⁶⁰, L. Mcconnell²¹, T.H. McGrath⁶¹, N.T. McHugh⁵⁸, A. McNab⁶¹, R. McNulty²¹, B. Meadows⁶⁴, G. Meier¹⁸, D. Melnychuk⁴⁰, F. M. Meng⁴, M. Merk⁴, A. Merli⁴⁸, L. Meyer Garcia⁶⁵, D. Miao^{5,7}, H. Miao⁷, M. Mikhasenko^{17,f}, D.A. Milanes⁷³, A. Minotti^{29,p}, E. Minucci⁶⁷, T. Miralles¹¹, B. Mitreska¹⁸, D.S. Mitzel¹⁸, A. Modak⁵⁶, A. Mödden¹⁸, R.A. Mohammed⁶², R.D. Moise¹⁶, S. Mokhnenko⁴², T. Mombächer⁴⁷, M. Monk^{1,55}, S. Monteil¹¹, A. Morcillo Gomez⁴⁵, G. Morello²⁶, M.J. Morello^{33,s}, M.P. Morgenthaler²⁰, A.B. Morris⁴⁷, A.G. Morris¹², R. Mountain⁶⁷, H. Mu⁴, Z. M. Mu⁶, E. Muhammad⁵⁵, F. Muheim⁵⁷, M. Mulder⁷⁵, K. Müller⁴⁹, F. Muñoz-Rojas⁹, R. Murta⁶⁰, P. Naik⁵⁹, T. Nakada⁴⁸, R. Nandakumar⁵⁶, T. Nanut⁴⁷, I. Nasteva³, M. Needham⁵⁷, N. Neri^{28,o}, S. Neubert¹⁷, N. Neufeld⁴⁷, P. Neustroev⁴², J. Nicolini^{13,18}, D. Nicotra⁷⁶, E.M. Niel⁴⁸, N. Nikitin⁴², P. Nogarolli³, P. Nogga¹⁷, N.S. Nolte⁶³, C. Normand⁵³, J. Novoa Fernandez⁴⁵, G. Nowak⁶⁴, C. Nunez⁸⁰, H. N. Nur⁵⁸, A. Oblakowska-Mucha³⁸, V. Obraztsov⁴², T. Oeser¹⁶, S. Okamura^{24,1,47}, A. Okhotnikov⁴², O. Okhrimenko⁵¹, R. Oldeman^{30,k}, F. Oliva⁵⁷, M. Olocco¹⁸, C.J.G. Onderwater⁷⁶, R.H. O’Neil⁵⁷, J.M. Otorola Goicochea³, P. Owen⁴⁹, A. Oyanguren⁴⁶, O. Ozcelik⁵⁷, K.O. Padeken¹⁷, B. Pagare⁵⁵, P.R. Pais²⁰, T. Pajero⁴⁷, A. Palano²², M. Palutan²⁶, G. Panshin⁴², L. Paolucci⁵⁵, A. Papanestis⁵⁶, M. Pappagallo^{22,h}, L.L. Pappalardo^{24,1}, C. Pappenheimer⁶⁴, C. Parkes⁶¹, B. Passalacqua²⁴, G. Passaleva²⁵, D. Passaro^{33,s}, A. Pastore²², M. Patel⁶⁰, J. Patoc⁶², C. Patrignani^{23,j}, A. Paul⁶⁷, C.J. Pawley⁷⁶, A. Pellegrino³⁶, J. Peng^{5,7}, M. Pepe Altarelli²⁶, S. Perazzini²³, D. Pereima⁴², A. Pereira Castro⁴⁵, P. Perret¹¹, A. Perro⁴⁷, K. Petridis⁵³, A. Petrolini^{27,n}, J. P. Pfaller⁶⁴, H. Pham⁶⁷, L. Pica^{33,s}, M. Piccini³², B. Pietrzyk¹⁰, G. Pietrzyk¹³, D. Pinci³⁴, F. Pisani⁴⁷, M. Pizzichemi^{29,p}, V. Placinta⁴¹, M. Plo Casaus⁴⁵, F. Polci^{15,47}, M. Poli Lener²⁶, A. Poluektov¹², N. Polukhina⁴², I. Polyakov⁴⁷, E. Polycarpo³, S. Ponce⁴⁷, D. Popov⁷, S. Poslavskii⁴², K. Prasanth⁵⁷, C. Prouve⁴⁵, V. Pugatch⁵¹, G. Punzi^{33,t}, S. Qasim⁴⁹, W. Qian⁷, N. Qin⁴, S. Qu⁴, R. Quagliani⁴⁷, R.I. Rabadan Trejo⁵⁵, J.H. Rademacker⁵³, M. Rama³³, M. Ramírez García⁸⁰, M. Ramos Pernas⁵⁵, M.S. Rangel³, F. Ratnikov⁴², G. Raven³⁷, M. Rebollo De Miguel⁴⁶, F. Redi^{28,i}, J. Reich⁵³, F. Reiss⁶¹, Z. Ren⁷, P.K. Resmi⁶², R. Ribatti^{33,s}, G. R. Ricart^{14,81}, D. Ricciardi^{33,s}, S. Ricciardi⁵⁶, K. Richardson⁶³, M. Richardson-Slipper⁵⁷, K. Rinnert⁵⁹, P. Robbe¹³, G. Robertson⁵⁸, E. Rodrigues⁵⁹, E. Rodriguez Fernandez⁴⁵, J.A. Rodriguez Lopez⁷³, E. Rodriguez Rodriguez⁴⁵, A. Rogovskiy⁵⁶, D.L. Roloff⁴⁷, P. Roloff⁴⁷, V. Romanovskiy⁴², M. Romero Lamas⁴⁵, A. Romero Vidal⁴⁵, G. Romolini²⁴, F. Ronchetti⁴⁸, M. Rotondo²⁶, S. R. Roy²⁰, M.S. Rudolph⁶⁷, T. Ruf⁴⁷, M. Ruiz Diaz²⁰, R.A. Ruiz Fernandez⁴⁵, J. Ruiz Vidal^{79,aa}, A. Ryzhikov⁴², J. Ryzka³⁸, J. J. Saavedra-Arias⁹, J.J. Saborido Silva⁴⁵, R. Sadek¹⁴, N. Sagidova⁴², D. Sahoo⁷⁴, N. Sahoo⁵², B. Saitta^{30,k}, M. Salomoni^{29,p,47}, C. Sanchez Gras³⁶, I. Sanderswood⁴⁶, R. Santacesaria³⁴, C. Santamarina Rios⁴⁵, M. Santimaria^{26,47}, L. Santoro², E. Santovetti³⁵, A. Saputi^{24,47}, D. Saranin⁴², G. Sarpis⁵⁷, M. Sarpis⁶¹, C. Satriano^{34,u}, A. Satta³⁵, M. Saur⁶, D. Savrina⁴², H. Sazak¹⁶, L.G. Scantlebury Smead⁶², A. Scarabotto¹⁸, S. Schael¹⁶

S. Scherl⁵⁹, M. Schiller⁵⁸, H. Schindler⁴⁷, M. Schmelling¹⁹, B. Schmidt⁴⁷, S. Schmitt¹⁶, H. Schmitz¹⁷, O. Schneider⁴⁸, A. Schopper⁴⁷, N. Schulte¹⁸, S. Schulte⁴⁸, M.H. Schune¹³, R. Schwemmer⁴⁷, G. Schwering¹⁶, B. Sciascia²⁶, A. Sciuccati⁴⁷, S. Sellam⁴⁵, A. Semennikov⁴², T. Senger⁴⁹, M. Senghi Soares³⁷, A. Sergi²⁷, N. Serra⁴⁹, L. Sestini³¹, A. Seuthe¹⁸, Y. Shang⁶, D.M. Shangase⁸⁰, M. Shapkin⁴², R. S. Sharma⁶⁷, I. Shchemerov⁴², L. Shchutska⁴⁸, T. Shears⁵⁹, L. Shekhtman⁴², Z. Shen⁶, S. Sheng^{5,7}, V. Shevchenko⁴², B. Shi⁷, Q. Shi⁷, E.B. Shields^{29,p}, Y. Shimizu¹³, E. Shmanin⁴², R. Shorkin⁴², J.D. Shupperd⁶⁷, R. Silva Coutinho⁶⁷, G. Simi^{31,q}, S. Simone^{22,h}, N. Skidmore⁵⁵, T. Skwarnicki⁶⁷, M.W. Slater⁵², J.C. Smallwood⁶², E. Smith⁶³, K. Smith⁶⁶, M. Smith⁶⁰, A. Snoch³⁶, L. Soares Lavra⁵⁷, M.D. Sokoloff⁶⁴, F.J.P. Soler⁵⁸, A. Solomin^{42,53}, A. Solovov⁴², I. Solovyev⁴², R. Song¹, Y. Song⁴⁸, Y. Song⁴, Y. S. Song⁶, F.L. Souza De Almeida⁶⁷, B. Souza De Paula³, E. Spadaro Norella^{28,o}, E. Spedicato²³, J.G. Speer¹⁸, E. Spiridenkov⁴², P. Spradlin⁵⁸, V. Sriskaran⁴⁷, F. Stagni⁴⁷, M. Stahl⁴⁷, S. Stahl⁴⁷, S. Stanislaus⁶², E.N. Stein⁴⁷, O. Steinkamp⁴⁹, O. Stenyakin⁴², H. Stevens¹⁸, D. Strelkina⁴², Y. Su⁷, F. Suljik⁶², J. Sun³⁰, L. Sun⁷², Y. Sun⁶⁵, D. Sundfeld², W. Sutcliffe⁴⁹, P.N. Swallow⁵², F. Swystun⁵⁴, A. Szabelski⁴⁰, T. Szumlak³⁸, Y. Tan⁴, M.D. Tat⁶², A. Terentev⁴², F. Terzuoli^{33,w}, F. Teubert⁴⁷, E. Thomas⁴⁷, D.J.D. Thompson⁵², H. Tilquin⁶⁰, V. Tisserand¹¹, S. T'Jampens¹⁰, M. Tobin⁵, L. Tomassetti^{24,l}, G. Tonani^{28,o,47}, X. Tong⁶, D. Torres Machado², L. Toscano¹⁸, D.Y. Tou⁴, C. Trippel⁴³, G. Tuci²⁰, N. Tuning³⁶, L.H. Uecker²⁰, A. Ukleja³⁸, D.J. Unverzagt²⁰, E. Urso⁴², A. Usachov³⁷, A. Ustyuzhanin⁴², U. Uwer²⁰, V. Vagnoni²³, A. Valassi⁴⁷, G. Valenti²³, N. Valls Canudas⁴⁷, H. Van Hecke⁶⁶, E. van Herwijnen⁶⁰, C.B. Van Hulse^{45,y}, R. Van Laak⁴⁸, M. van Veghel³⁶, G. Vasquez⁴⁹, R. Vazquez Gomez⁴⁴, P. Vazquez Regueiro⁴⁵, C. Vázquez Sierra⁴⁵, S. Vecchi²⁴, J.J. Velthuis⁵³, M. Veltri^{25,x}, A. Venkateswaran⁴⁸, M. Vesterinen⁵⁵, M. Vieites Diaz⁴⁷, X. Vilasis-Cardona⁴³, E. Vilella Figueras⁵⁹, A. Villa²³, P. Vincent¹⁵, F.C. Volle⁵², D. vom Bruch¹², N. Voropaev⁴², K. Vos⁷⁶, G. Vouters^{10,47}, C. Vrahas⁵⁷, J. Wagner¹⁸, J. Walsh³³, E.J. Walton^{1,55}, G. Wan⁶, C. Wang²⁰, G. Wang⁸, J. Wang⁶, J. Wang⁵, J. Wang⁴, J. Wang⁷², M. Wang²⁸, N. W. Wang⁷, R. Wang⁵³, X. Wang⁸, X. Wang⁷⁰, X. W. Wang⁶⁰, Z. Wang¹³, Z. Wang⁴, Z. Wang²⁸, J.A. Ward^{1,55}, M. Waterlaet⁴⁷, N.K. Watson⁵², D. Websdale⁶⁰, Y. Wei⁶, J. Wendel⁷⁸, B.D.C. Westhenry⁵³, D.J. White⁶¹, M. Whitehead⁵⁸, A.R. Wiederhold⁵⁵, D. Wiedner¹⁸, G. Wilkinson⁶², M.K. Wilkinson⁶⁴, M. Williams⁶³, M.R.J. Williams⁵⁷, R. Williams⁵⁴, F.F. Wilson⁵⁶, W. Wislicki⁴⁰, M. Witek³⁹, L. Witola²⁰, C.P. Wong⁶⁶, G. Wormser¹³, S.A. Wotton⁵⁴, H. Wu⁶⁷, J. Wu⁸, Y. Wu⁶, Z. Wu⁷, K. Wyllie⁴⁷, S. Xian⁷⁰, Z. Xiang⁵, Y. Xie⁸, A. Xu³³, J. Xu⁷, L. Xu⁴, L. Xu⁴, M. Xu⁵⁵, Z. Xu¹¹, Z. Xu⁷, Z. Xu⁵, D. Yang, S. Yang⁷, X. Yang⁶, Y. Yang^{27,n}, Z. Yang⁶, Z. Yang⁶⁵, V. Yeroshenko¹³, H. Yeung⁶¹, H. Yin⁸, C. Y. Yu⁶, J. Yu⁶⁹, X. Yuan⁵, E. Zaffaroni⁴⁸, M. Zavertyaev¹⁹, M. Zdybal³⁹, C. Zeng^{5,7}, M. Zeng⁴, C. Zhang⁶, D. Zhang⁸, J. Zhang⁷, L. Zhang⁴, S. Zhang⁶⁹, S. Zhang⁶, Y. Zhang⁶, Y. Z. Zhang⁴, Y. Zhao²⁰, A. Zharkova⁴², A. Zhelezov²⁰, X. Z. Zheng⁴, Y. Zheng⁷, T. Zhou⁶, X. Zhou⁸, Y. Zhou⁷, V. Zhovkovska^{55,*}, L. Z. Zhu⁷, X. Zhu⁴, X. Zhu⁸, V. Zhukov¹⁶, J. Zhuo⁴⁶, Q. Zou^{5,7}, D. Zuliani^{31,q}, G. Zunica⁴⁸

¹ School of Physics and Astronomy, Melbourne, Australia

² Centro Brasileiro de Pesquisas Físicas (CBPF), Rio de Janeiro, Brazil

³ Universidade Federal do Rio de Janeiro (UFRJ), Rio de Janeiro, Brazil

⁴ Center for High Energy Physics, Tsinghua University, Beijing, China

⁵ Institute of High Energy Physics (IHEP), Beijing, China

⁶ School of Physics State Key Laboratory of Nuclear Physics and Technology, Peking University, Beijing, China

⁷ University of Chinese Academy of Sciences, Beijing, China

⁸ Institute of Particle Physics, Central China Normal University, Wuhan, Hubei, China

⁹ Consejo Nacional de Rectores (CONARE), San Jose, Costa Rica

¹⁰ Université Savoie Mont Blanc, CNRS, IN2P3-LAPP, Annecy, France

¹¹ Université Clermont Auvergne, CNRS/IN2P3, LPC, Clermont-Ferrand, France

¹² Aix Marseille Univ, CNRS/IN2P3, CPPM, Marseille, France

¹³ University of Warwick and Université Paris-Saclay, CNRS/IN2P3, IJCLab, Orsay, France

¹⁴ Laboratoire Leprince-Ringuet, CNRS/IN2P3, Ecole Polytechnique, Institut Polytechnique de Paris, Palaiseau, France

¹⁵ LPNHE, Sorbonne Université, Paris Diderot Sorbonne Paris Cité, CNRS/IN2P3, Paris, France

¹⁶ I. Physikalisches Institut, RWTH Aachen University, Aachen, Germany

¹⁷ Universität Bonn - Helmholtz-Institut für Strahlen und Kernphysik, Bonn, Germany

- 18 Fakultät Physik, Technische Universität Dortmund, Dortmund, Germany
- 19 Max-Planck-Institut für Kernphysik (MPIK), Heidelberg, Germany
- 20 Physikalisches Institut, Ruprecht-Karls-Universität Heidelberg, Heidelberg, Germany
- 21 School of Physics, University College Dublin, Dublin, Ireland
- 22 INFN Sezione di Bari, Bari, Italy
- 23 INFN Sezione di Bologna, Bologna, Italy
- 24 INFN Sezione di Ferrara, Ferrara, Italy
- 25 INFN Sezione di Firenze, Firenze, Italy
- 26 INFN Laboratori Nazionali di Frascati, Frascati, Italy
- 27 INFN Sezione di Genova, Genova, Italy
- 28 INFN Sezione di Milano, Milan, Italy
- 29 INFN Sezione di Milano-Bicocca, Milan, Italy
- 30 INFN Sezione di Cagliari, Monserrato, Italy
- 31 INFN Sezione di Padova, Padua, Italy
- 32 INFN Sezione di Perugia, Perugia, Italy
- 33 INFN Sezione di Pisa, Pisa, Italy
- 34 INFN Sezione di Roma La Sapienza, Rome, Italy
- 35 INFN Sezione di Roma Tor Vergata, Rome, Italy
- 36 Nikhef National Institute for Subatomic Physics, Amsterdam, The Netherlands
- 37 Nikhef National Institute for Subatomic Physics and VU University Amsterdam, Amsterdam, The Netherlands
- 38 Faculty of Physics and Applied Computer Science, AGH-University of Krakow, Kraków, Poland
- 39 Henryk Niewodniczanski Institute of Nuclear Physics Polish Academy of Sciences, Kraków, Poland
- 40 National Center for Nuclear Research (NCBJ), Warsaw, Poland
- 41 Horia Hulubei National Institute of Physics and Nuclear Engineering, Bucharest-Magurele, Romania
- 42 Affiliated with an Institute Covered by a Cooperation Agreement with CERN, Geneva, Switzerland
- 43 DS4DS, La Salle, Universitat Ramon Llull, Barcelona, Spain
- 44 ICCUB, Universitat de Barcelona, Barcelona, Spain
- 45 Instituto Galego de Física de Altas Enerxías (IGFAE), Universidade de Santiago de Compostela, Santiago de Compostela, Spain
- 46 Instituto de Física Corpuscular, Centro Mixto Universidad de Valencia - CSIC, Valencia, Spain
- 47 European Organization for Nuclear Research (CERN), Geneva, Switzerland
- 48 Institute of Physics, Ecole Polytechnique Fédérale de Lausanne (EPFL), Lausanne, Switzerland
- 49 Physik-Institut, Universität Zürich, Zürich, Switzerland
- 50 NSC Kharkiv Institute of Physics and Technology (NSC KIPT), Kharkiv, Ukraine
- 51 Institute for Nuclear Research of the National Academy of Sciences (KINR), Kyiv, Ukraine
- 52 School of Physics and Astronomy, University of Birmingham, Birmingham, UK
- 53 H.H. Wills Physics Laboratory, University of Bristol, Bristol, UK
- 54 Cavendish Laboratory, University of Cambridge, Cambridge, UK
- 55 Department of Physics, University of Warwick, Coventry, UK
- 56 STFC Rutherford Appleton Laboratory, Didcot, UK
- 57 School of Physics and Astronomy, University of Edinburgh, Edinburgh, UK
- 58 School of Physics and Astronomy, University of Glasgow, Glasgow, UK
- 59 Oliver Lodge Laboratory, University of Liverpool, Liverpool, UK
- 60 Imperial College London, London, UK
- 61 Department of Physics and Astronomy, University of Manchester, Manchester, UK
- 62 Department of Physics, University of Oxford, Oxford, UK
- 63 Massachusetts Institute of Technology, Cambridge, MA, USA
- 64 University of Cincinnati, Cincinnati, OH, USA
- 65 University of Maryland, College Park, MD, USA
- 66 Los Alamos National Laboratory (LANL), Los Alamos, NM, USA
- 67 Syracuse University, Syracuse, NY, USA
- 68 Pontifícia Universidade Católica do Rio de Janeiro (PUC-Rio), Rio de Janeiro, Brazil, associated to ³
- 69 School of Physics and Electronics, Hunan University, Changsha, China, associated to ⁸

- ⁷⁰ Guangdong Provincial Key Laboratory of Nuclear Science, Guangdong-Hong Kong Joint Laboratory of Quantum Matter, Institute of Quantum Matter, South China Normal University, Guangzhou, China, associated to ⁴
- ⁷¹ Lanzhou University, Lanzhou, China, associated to ⁵
- ⁷² School of Physics and Technology, Wuhan University, Wuhan, China associated to ⁴
- ⁷³ Departamento de Física, Universidad Nacional de Colombia, Bogota, Colombia, associated to ¹⁵
- ⁷⁴ Eotvos Lorand University, Budapest, Hungary, associated to ⁴⁷
- ⁷⁵ Van Swinderen Institute, University of Groningen, Groningen, The Netherlands, associated to ³⁶
- ⁷⁶ Universiteit Maastricht, Maastricht, The Netherlands, associated to ³⁶
- ⁷⁷ Tadeusz Kosciuszko Cracow University of Technology, Cracow, Poland, associated to ³⁹
- ⁷⁸ Universidade da Coruña, A Coruna, Spain associated to ⁴³
- ⁷⁹ Department of Physics and Astronomy, Uppsala University, Uppsala, Sweden, associated to ⁵⁸
- ⁸⁰ University of Michigan, Ann Arbor, MI, USA, associated to ⁶⁷
- ⁸¹ Departement de Physique Nucleaire (SPhN), Gif-Sur-Yvette, France
- ^a Universidade de Brasília, Brasília, Brazil
- ^b Centro Federal de Educação Tecnológica Celso Suckow da Fonseca, Rio De Janeiro, Brazil
- ^c Hangzhou Institute for Advanced Study, UCAS, Hangzhou, China
- ^d School of Physics and Electronics, Henan University, Kaifeng, China
- ^e LIP6, Sorbonne Université, Paris, France
- ^f Excellence Cluster ORIGINS, Munich, Germany
- ^g Universidad Nacional Autónoma de Honduras, Tegucigalpa, Honduras
- ^h Università di Bari, Bari, Italy
- ⁱ Università di Bergamo, Bergamo, Italy
- ^j Università di Bologna, Bologna, Italy
- ^k Università di Cagliari, Cagliari, Italy
- ^l Università di Ferrara, Ferrara, Italy
- ^m Università di Firenze, Firenze, Italy
- ⁿ Università di Genova, Genova, Italy
- ^o Università degli Studi di Milano, Milan, Italy
- ^p Università degli Studi di Milano-Bicocca, Milan, Italy
- ^q Università di Padova, Padua, Italy
- ^r Università di Perugia, Perugia, Italy
- ^s Scuola Normale Superiore, Pisa, Italy
- ^t Università di Pisa, Pisa, Italy
- ^u Università della Basilicata, Potenza, Italy
- ^v Università di Roma Tor Vergata, Rome, Italy
- ^w Università di Siena, Siena, Italy
- ^x Università di Urbino, Urbino, Italy
- ^y Universidad de Alcalá, Alcalá de Henares, Spain
- ^z Facultad de Ciencias Físicas, Madrid, Spain
- ^{aa} Department of Physics/Division of Particle Physics, Lund, Sweden
- [†] Deceased